Available online at www.sciencedirect.com

ScienceDirect

Geochimica et Cosmochimica Acta 284 (2020) 134–155

Geochimica et Cosmochimica Acta

www.elsevier.com/locate/gca

Sedimentary vanadium isotope signatures in low oxygen marine conditions

Fei Wu [a,b,*], Jeremy D. Owens [b], Florian Scholz [c], Linqing Huang [d], Siqi Li [b], Natascha Riedinger [e], Larry C. Peterson [f], Christopher R. German [g], Sune G. Nielsen [g,h]

[a] Department of Earth and Environmental Sciences, Macquarie University, Sydney, New South Wales 2109, Australia
[b] Department of Earth, Ocean and Atmospheric Science and National High Magnet Field Laboratory, Florida State University, Tallahassee, FL, USA
[c] GEOMAR Helmholtz Centre for Ocean Research Kiel, Wischhofstraße 1-3, 24111 Kiel, Germany
[d] Scripps Institution of Oceanography, University of California San Diego, San Diego, CA 92037, USA
[e] Boone Pickens School of Geology, Oklahoma State University, 74078 Stillwater, OK, USA
[f] Rosenstiel School of Marine and Atmospheric Science, University of Miami, Miami, FL 33149, USA
[g] Department of Geology and Geophysics, Woods Hole Oceanographic Institution, Woods Hole, MA, USA
[h] NIRVANA Laboratories, Woods Hole Oceanographic Institution, Woods Hole, MA, USA

Received 2 December 2019; accepted in revised form 11 June 2020; available online 20 June 2020

Abstract

It has been hypothesized that vanadium (V) isotopes have the potential to track sedimentary redox conditions due to multiple valence states occurring in nature, which might induce variable V isotope fractionation as a function of sedimentary redox state. These characteristica could make V isotopes a useful paleo-redox proxy. However, in order to understand the mechanisms driving V isotope fractionation, it is crucial to build a framework for the depositional and post-depositional controls on sedimentary V isotope records from a diverse set of sedimentary environments. This study, for the first time, investigates the V isotope variations of modern marine sediments deposited under a range of redox environments. Our results document that changes in local redox conditions impart a significant isotopic fractionation from seawater as recorded in the local sedimentary V isotopic signature. Importantly, there is a significant difference between the V isotope composition of sediments deposited in the open ocean setting with oxygen-deficient bottom waters compared to less reducing environments, whereby oxic sediments (benthic oxygen contents > 10 μM) exhibit $\Delta_{oxic} = -1.1 \pm 0.3$‰ and anoxic sediments exhibit $\Delta_{anoxic} = -0.7 \pm 0.2$‰. Combined with previous studies on seawater particulate and sediment pore fluid analysis, our results indicate that V is mainly delivered and enriched in anoxic sediments through settling particulates. Authigenic V isotope compositions in marine sediments are likely controlled by isotope fractionation between V species bound to particulates and dissolved in seawater, which likely varies with the speciation and adsorption properties of V that are strongly controlled by local redox conditions. In addition, the euxinic Cariaco Basin sediments exhibit distinctive $\Delta_{euxinic} = -0.4 \pm 0.2$‰, which is likely influenced by the relationship between the seawater V removal rate and the seawater renewal rate. Our results highlight the direct link between authigenic marine sedimentary V isotope compositions and the overlying local redox conditions. This investigation of V isotopes in modern marine environments provides an initial framework for the utilization of V isotopes

* Corresponding author at: Department of Earth and Environmental Sciences, Macquarie University, Sydney, New South Wales 2109, Australia.
E-mail address: fei.wu@mq.edu.au (F. Wu).

https://doi.org/10.1016/j.gca.2020.06.013

to reconstruct ancient redox fluctuations, which has the potential to track subtle redox variations of local oxygen-deficient to low oxygen environments.

Keywords: V isotope; Isotope fractionation; Stable isotopes; Redox; Suboxic sediments

1. INTRODUCTION

Reconstructing marine redox conditions is critical for understanding Earth system feedbacks and the evolution of life (e.g. Meyer and Kump, 2008; Mills et al., 2014; Sperling et al., 2015; Reinhard et al., 2016). Over the last several decades, there has been significant development and application of various geochemical redox proxies. For instance, the relative abundances of transition metals referred to as redox-sensitive trace elements (e.g., Cr, Mo, U, Re, V) in marine sediments have been used to reconstruct the local and global redox state of the ancient oceans (e.g. Algeo and Tribovillard, 2009; Crusius et al., 1996; McManus et al., 2006; Scott and Lyons, 2012; Tribovillard et al., 2006). Geochemical studies of past ocean redox conditions have also utilized isotopic proxies of redox relative elements like Mo, U, Cr, and Tl in marine record (e.g. Anbar and Rouxel, 2007; Andersen et al., 2014; Kendall et al., 2017; Owens et al., 2017). In addition, iron-speciation geochemistry has been used to discern local redox conditions: it has been applied to infer reducing conditions, and to further delineate the type of anoxic conditions as ferruginous or euxinic (sulfidic water column) in local water masses (e.g. Poulton and Canfield, 2011; Raiswell et al., 2018; Scholz, 2018). These proxies have broad spatiotemporal applications and provide a wealth of information about redox geochemical fingerprints and the evolution of ancient oceans.

Despite the significant developments in establishing paleoredox proxies, our current geochemical tools lack the specificity to track subtle changes of benthic low oxygen conditions in ancient oceans, because current geochemical redox proxies typically operate below redox conditions defined by the oxic-anoxic boundary (e.g. Owens, 2019). Multiple modern studies have demonstrated that the marine benthic biological community is highly sensitive to oxygen variations at low but non-zero concentrations (e.g. Levin, 2003; Sperling et al., 2015). Furthermore, a study by Sperling et al. (2013) shows that the abundance, size, and diversity of marine carnivory is highly sensitive to subtle benthic oxygen variations in OMZs (oxygen minimum zones). Thus, a low oxygen redox proxy is required to better understand the interrelation among climatic perturbations, ocean chemistry, and the existence, evolution, extinction, and recovery of marine animals in Earth's history.

Vanadium is a multi-valence element that occurs as penta-, tetra-, or tri- valent species at standard Earth surface conditions. In modern seawater, V concentrations vary from ~30 to 40 nmol/L, with a currently calculated marine residence time of ~50–100 kyrs and homogeneous reservoir in the deep ocean (Collier, 1984; Jeandel et al., 1987; Shiller and Boyle, 1987; Ho et al., 2018). The geochemical cycle of V in the oceans is mainly controlled by the local redox conditions, which dictate the valence state of the species and thus the solubility of V in seawater (e.g., Morford and Emerson, 1999; Algeo and Maynard, 2004). Under oxic conditions, V mainly occurs as a pentavalent species, vanadate (e.g. HVO_4^{2-} and $H_2VO_4^-$), that is highly soluble in seawater. Vanadate can be adsorbed onto Fe-Mn (oxyhydr) oxide and clay minerals in marine sediments (e.g. Wehrli and Stumm, 1989; Morford and Emerson, 1999). Under mildly reducing conditions, dissolved vanadate tends to be reduced to the tetravalent species vanadyl (e.g. VO^{2+}, $VO(OH)_3^+$) by organic compounds, which is likely to coprecipitate with minerals and organic substances (Breit and Wanty, 1991; Algeo and Maynard, 2004). Under more strongly reducing conditions, vanadyl might be further reduced to the highly insoluble trivalent V species by free H_2S in the water column or pore fluids and directly precipitate as a solid oxide or hydroxide (Wanty and Goldhaber, 1992). The redox potential of the V(V)-V(IV) pair is close to that of NO_3^-–NO_2^-/NH_4^+ and higher than that of Fe (III)-Fe (II) in seawater (e.g. Bonatti et al., 1971; Algeo and Li, 2020), thus the reduction and sequestration of V from seawater begins under low oxygen conditions. Previous studies also showed that the enrichment of V in sediments starts under less reducing conditions than that required for the enrichment of metals with a greater affinity toward sulfide, such as Mo (Algeo and Maynard, 2004; Tribovillard et al., 2006). Thus, these data suggest that the geochemical cycle of V is more sensitive to subtle changes in benthic oxygen levels than other available redox proxies (e.g. Mo, Fe, S, U). Several studies have applied variations in the V content of sediments to track changes in local bottom redox conditions (e.g. Han et al., 2018; Filippidi and De Lange, 2019) and on global scales (e.g. Sahoo et al., 2012, 2016; Owens et al., 2016). Nonetheless, a variety of interlinked factors have been proposed to play a role in the magnitude of trace metal enrichment in sediments, which includes the marine trace metal inventory, the local redox state, the sinking rate of organic carbon, the input flux of terrigenous materials, as well as local sedimentation rates (e.g. Nameroff et al., 2002; Algeo, 2004; McManus et al., 2006; Scholz et al., 2011). Importantly, sedimentation rates can vary significantly over time and likely change during major climatic events (e.g. Piper and Calvert, 2009). Considering the high abundance of V in the upper continental crust (~97 μg/g, Rudnick and Gao, 2013), the background detrital delivery of V could be variable during major climatic events. For these reasons, minor ancient V enrichments are difficult to interpret as a direct paleo-redox proxy.

Vanadium has two stable isotopes, ^{50}V (~0.25%) and ^{51}V (~99.75%). Recent advances in the chemical separation and purification, and high-precision isotopic measurements

using a multi-collector inductively coupled plasma mass-spectrometer (MC-ICP-MS) have allowed even small natural isotopic variations in V to be analytically resolved (Nielsen et al., 2011, 2016; Prytulak et al., 2011; Wu et al., 2016; Schuth et al., 2017). A V isotope study on seawater suggested that the global V isotope composition of seawater is homogeneous with $\delta^{51}V = +0.20 \pm 0.15‰$ (Wu et al., 2019a). For comparison, current V isotope data of river waters shows dissoved $\delta^{51}V = -0.50 \pm 0.20‰$ (Schuth et al., 2019), thus indicating the occurrence of isotope fractionation during V removal from seawater as the river input and seawater value are significantly different. Furthermore, a recent study documented that hydrogenetic Fe-Mn crusts show V isotope composirion ($-1.05 \pm 0.16‰$) much lighter compared to seawater, thus indicateing that a large V isotope fractionation occurs during the adsorption of V onto marine Fe-Mn crusts (Wu et al., 2019b). Lastly, published theoretical calculations suggest that there is significant V isotope fractionation between V species with different valences and chemical bonding environments, thus isotopic fractionation during the uptake of V from seawater can be expected to vary with local redox conditions (Wu et al., 2015). Therefore, the V isotope system potentially provides additional geochemical evidence for marine redox conditions, with the specificity of constraining the variations of non-sulfidic but oxygen-deficient seafloor areas (Tyson and Pearson, 1991), referred to as suboxic condition.

The first step required in order to apply V isotopes as a new proxy for the reconstruction of paleo-ocean redox conditions is a comprehensive investigation of the V isotope composition of modern marine sediments deposited under variable redox conditions. Additionally, it is critical to establish the depositional and post-depositional controls on sedimentary V isotope records from a diverse set of sedimentary environments. Although significant isotope variations of V in supergene deposits have been predicted by theoretical calculation and documented in natural observation, modern marine sediments have not been explored beyond ferromanganese nodules and crusts. In this work, we investigate the V isotope variations of sediments deposited under various redox environments that range from oxic, oxygen-deficient, anoxic, and euxinic conditions. Our data suggest that there is strong linkage between the sedimentary V isotope composition and the environmental redox conditions. This work further provides the foundation for the interpretation of the observed V isotope variations in modern sediments as it continues to build the framework for the marine V isotope mass balance, and eventual application of V isotopes as a paleo-redox proxy in marine sediments to track subtle redox variations of low oxygen environments.

2. SAMPLE LOCALITIES AND BACKGROUND

Twenty-two pelagic sediment samples from various localities around the globe were investigated in this study (Fig. 1). A total of thirteen samples were analyzed from the Pacific Ocean at water depths of 3500–5800 m, four samples were analyzed from the Indian Ocean at water depths of 4400–5200 m, four samples were analyzed from the Atlantic Ocean at water depths of 3300–6000 m, and one sample was analyzed from the Arctic Ocean at water depths of 4041 m. All the samples are distal from any known marine hydrothermal vent field and thus should not include a hydrothermal signature. Sediment lithologies consist predominantly of oxidized fine-grained pelagic clay ranging from light to dark brown or greenish-gray in color, with various carbonate and calcareous ooze contents. Dried sediments were collected from cores housed in the sediment repository of Woods Hole Oceanographic Institution (WHOI) and from the U.S. GEOTRACES East Pacific Zonal Transect (EPZT GP16). These samples are bulk powders from the top sections (0–10 cm) of cores.

Sediment samples from the continental margin off Namibia in the eastern South Atlantic were collected as part of the RV Meteor expeditions M57/2 (Fig. 1). The Benguela upwelling supplies cold and nutrient-rich deep waters to the euphotic zone in this area, which maintains intense primary production (Shannon and Nelson, 1996). The core samples were collected on a continental slope transect with water depths between 605 and 2470 m. The bottom water oxygen contents of the sample locations are from 150 to 220 μM (Table 1). The sediments in the Eastern Cape Basin are characterized by low input of terrigenous matter and high biogenic contents. The high amounts of organic matter (up to 9% for the analyzed V isotope sites) in the sediments are due to high water column primary production on the shelf and lateral transport of organic carbon from the shelf to the slope an (Inthorn et al., 2006; Abshire et al., 2020). The sediments off Namibia analyzed here are all core top sediments from 0 to 5 cm.

Sediment samples from the Argentine Basin in the western South Atlantic were collected during R/V Meteor expedition M78/3 (Krastel and Wefer, 2012). The confluence of the Brazil–Malvinas Currents in front of the Rio de la Plata results in strong gradients in nutrient, salinity, and temperature at this locality (Peterson and Stramma, 1991; Chiessi et al., 2007). Furthermore, the mixing of these tropical and Antarctic water masses causes an increase in primary production and thus elevated organic carbon input into the sediment along the shelf and upper slope of the Argentine Basin. The predominantly terrigenous material in this region is delivered from the numerous fluvial tributaries along the coast of Argentina and Uruguay and transported further downslope via gravity-controlled mass flows (Krastel et al., 2011). The core samples were collected east of the Rio de la Plata mouth from water depths between 58 m and 4273 m, forming a transect from shelf to deep basin. The geographical position and bottom water oxygen content of all sampling stations are summarized in Table 1. The sediments from the Argentine Basin analysis here are from core depths between 5 to 45 cm.

Samples from the Peruvian Margin in this study were mostly from a transect along 11°S during the RV Meteor cruise M77-1 in November 2008. In addition, some Peruvian Margin sediment samples were collected during the U.S. GEOTRACES East Pacific Zonal Transect (EPZT GP16) and R/V Moana Wave cruise 87 leg 08 (PUBS I) (Fig. 1). In this area, strong offshore Ekman transport along the western edge of South America leads to coastal upwelling

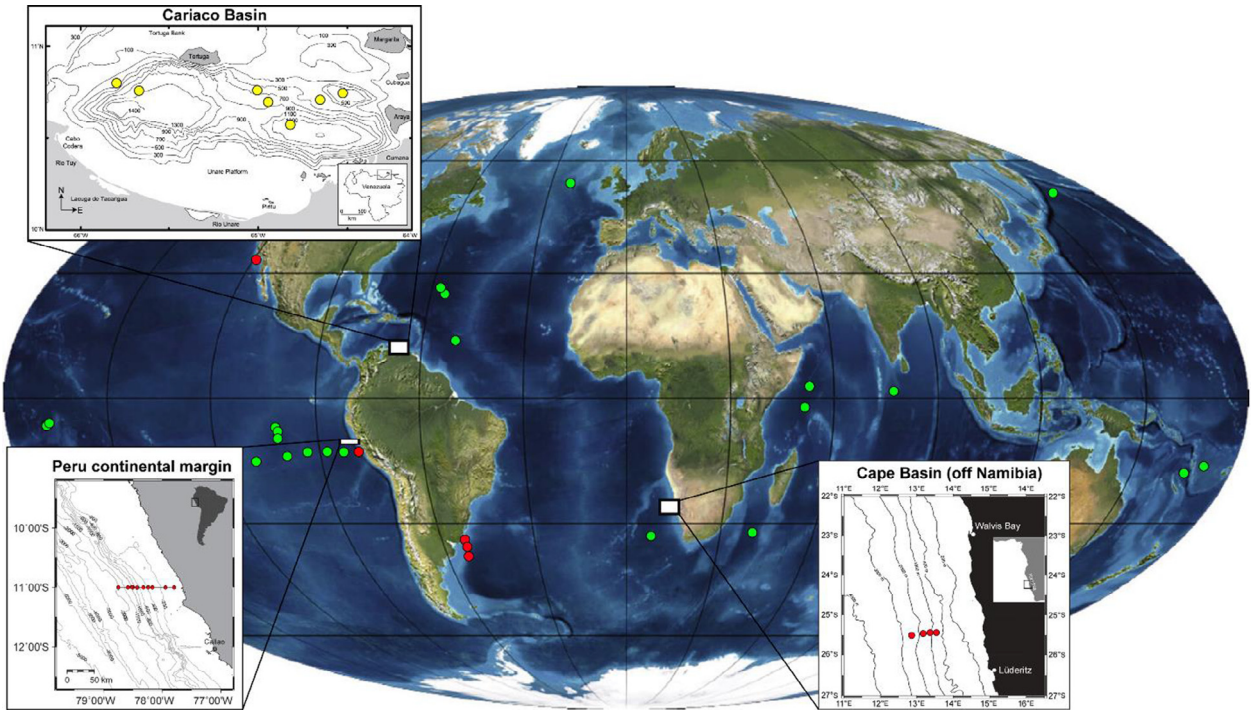

Fig. 1. Geographical location maps of samples investigated in this study. Green dot in the map shows locations of pelagic sediments in global oceans. Red dot in the map shows locations of continental margin sediments. Cariaco Basin inset with yellow dot documents core-top sediment sample locations. Inset of the Peruvian continental margin and Cape Basin off Namibia show the location of sediment samples. (For interpretation of the references to colour in this figure legend, the reader is referred to the web version of this article.)

of cold and nutrient-rich waters from the upper thermocline, which enables high primary productivity as well as high rates of subsurface and sedimentary organic matter degradation (Pennington et al., 2006). Thus, high oxygen demand within the water column leads to a perennial oxygen minimum zone (OMZ) that impinges on the continental shelf/slope between ~50 and 500 m water depth (Suess and von Huene, 1988; Fuenzalida et al., 2009; Scholz et al., 2011). Thirteen sediment cores were analyzed from the continental shelf to deep slope at water depths between 85 and 2025 m, which transects from the reducing OMZ to the deeper oxic seafloor with bottom water oxygen contents from <1.5 μM to 93.4 μM (Table 1). The Peruvian Margin samples analyzed were from core depths between 0 to 35 cm.

Sediment samples from the deepest portion (594 m water depth) of the Santa Barbara Basin were collected in 2001 as part of the CALMEX cruise (R/V New Horizon in November 2001). The Santa Barbara Basin is a shallow, near-shore basin off southern California with a sill depth of approximately 475 m (Bernhard and Reimers, 1991). Below the basin sill depth of 475 m, the water column is characterized by limited exchange with waters outside of the basin, thus the circulation within the basin is restricted resulting in low bottom water oxygen concentrations, typically < 5 μM (Zheng et al., 2000), though the concentration can vary on seasonal timescales (Sholkovitz, 1973; Reimers et al., 1996; Moffitt et al., 2014). The sedimentation rates in this basin are generally high, where ~2000 years is represented in 200 cm (Reimers et al., 1990; Zheng et al., 2000; Schimmelmann et al., 2013). The core samples were collected at the center of the basin with bottom water oxygen contents near-zero (~1 μM) (Bernhard et al., 1997) (Table 1). The Santa Barbara Basin samples analyzed here include the core top sediment (0–3 cm) to shallow depths (10–11 cm).

Sediment samples from the Cariaco Basin were collected in 1990 as part of the PLUME Leg 7 Cruise (R/V Thomas Washington) (Peterson et al., 1990). The Cariaco Basin is the second-largest euxinic (anoxic and sulfidic water column) marine basin in the modern ocean, covering an approximate area of 7000 km^2 within a structural depression on the continental shelf north of Venezuela. Seawater exchange with the Caribbean Sea is limited by the presence of shallow sills on the western (146 m depth) and northern basin margins (120 m depth). Below ~300 m water depth, the basin is euxinic due to a combination of limited deep-water renewal and high surface productivity supplying organic matter that promotes microbial respiration, oxygen depletion, and the accumulation of hydrogen sulfide (e.g. Scranton et al., 2001). Seven separate box core top samples (0–1 cm) from around the Cariaco basin including both sub-basins were collected (Fig. 1 and Table 1). All of the Cariaco sediment samples measured in this study were collected below the permanent chemocline (sulfidic portion) at water depths between 400 and 1350 m.

3. METHODS

3.1. Sample dissolution

Samples were dissolved using bulk digestion and leaching methods. Both methods were carried out to ensure that

Table 1
Summary of study site characteristics.

	Latitude	Longitude	Water depth m	BW O_2 μM
Cape Basin (off Namibia)				
8449–1	25°28.8′S	13°33.0′E	605	165
8451–1	25°28.8′S	13°21.6′E	1028	167
8455–1	25°30.6′S	13°10.8′E	1503	221
8470–1	25°33.0′S	12°51.6′E	2470	187
Argentine Basin				
13813–1	34°44.21′ S	53°33.29′ W	58	250
13809–2	36°07.67′ S	52°49.90′ W	1398	180
13819–4	39°29.44′ S	53°42.56′ W	4273	216
Peruvian margin				
BIGO-05	11°00.02′S	77°47.72′W	85	<1.5
MUC29	11°00.00′S	77°56.61′W	145	<1.5
MW87/08 SC02	11°04.21′S	78°03.14′W	255	<1.5
MUC19	11°00.01′S	78°09.97′W	319	<1.5
MUC33	11°00.00′S	78°14.19′W	376	<1.5
MUC21	11°00.01′S	78°19.24′W	465	2.1
MW87/08 SC06	15°11.49′S	75°34.51′W	535	~9
MUC25	11°00.03′S	78°25.60′W	697	12.1
EPZT MC4	12°02.69′S	77°49.09′W	770	13
MUC15	10°59.98′S	78°30.02′W	930	39.9
MUC53	10°59.99′S	78°31.27′W	1005	41.6
MUC26	11°00.01′S	78°35.11′W	1242	63.8
MUC27	11°00.01′S	78°44.76′W	2025	93.4
Santa Barbara Basin				
NH01 G6C-47	34°13.57′N	120°1.82′W	594	~1
Cariaco Basin				
PL07-22BX	10°52.2′N	65°10.2′W	656	0
PL07-89BX	10°39.6′N	64°51.6′W	1342	0
PL07-82BX	10°41.4′N	64°58.2′W	818	0
PL07-105BX	10°46.2′N	65°39.0′W	1296	0
PL07-67BX	10°41.3′N	64°39.3′W	400	0
PL07-69BX	10°46.2′N	64°36.6′W	545	0
PL07-111BX	10°50.4′N	65°46.8′W	411	0

BW is bottom water. References: Zabel (2003), Krastel and Wefer (2012), Scholz et al. (2011), McCaffrey et al. (1990).

the V isotope analyses captured the authigenic values, especially given the limited enrichment for some of the samples (e.g. differences between the bulk and leach methods). For the bulk digestion, sediment samples for V isotope analysis were ashed overnight at 600 °C to remove organic phases. Ashed sediment powders were then completely digested with a multi-acid HF–HNO_3–HCl procedure using trace metal clean acids. All materials were completely dissolved in 0.8 N HNO_3 prior to purification using ion exchange column chemistry.

Leach (also termed partial digestion) techniques were applied to extract authigenic V. For the organic carbon-rich sediments, splits of sediment were leached in a Teflon Savillex vial with 3 mL of 3 N HNO_3 for 12–16 hours at room temperature with constant agitation using a shaking table. These samples were then centrifuged, and the supernatant was collected and placed in a new clean Savillex vial and dried. During the collection of the supernatant, care was taken to avoid the solid phase siliciclastic materials; additionally, HF was avoided to ensure the limited dissolution of siliciclastic minerals. Several high-purity acid treatments (aqua regia, conc. HNO_3) were added to each vial to completely oxidize any organic matter that might have been present. Samples were then dissolved with 0.8 N HNO_3 prior to ion exchange column chemistry. To validate this leaching method, the leaching method was performed on United States Geological Survey (USGS) shale standards SCo-1 and SDO-1 with various HNO_3 concentrations (from 1 N to 5 N) at two different reaction temperatures (room temperature or 'cool leach' and 130 °C or 'hot leach'). Splits of the leach solution were also taken for elemental analysis. The details for above tests are discussed further in Section 5.1.

For the oxic pelagic sediments, we applied the well-established extraction technique for oxide dissolution to obtain the isotopic analysis of the authigenic V (Chester and Hughes, 1967). One aliquot of the pelagic sediments was reacted in 10 mL 25% acetic acid + 1 N hydroxylamine hydrochloride solution at 90℃ for three hours, and each sample was agitated every 30 minutes. The supernatant was removed from the detrital particles, treated with 8 N HNO_3 and then dissolved with 0.8 N HNO_3 prior to ion exchange column chemistry.

Table 2
Vanadium isotope compositions of reference materials.

	$\delta^{51}V$	2SD	Analyses	Splits	Reference
BCR-2	−0.74	0.08	2	1	This study
	−0.75	0.05	3	1	Qi et al. (2019)
	−0.71	0.15	24	10	Nielsen et al. (2019)
	−0.85	0.26	5	2	Hopkins et al. (2019)
	−1.11	0.08	2	1	Sossi et al. (2018)
	−1.03	0.09	9	n.g.	Schuth et al. (2017)
	−0.78	0.08	36	n.g.	Wu et al. (2016)
	−0.95	0.16	27	12	Prytulak et al. (2011)
AGV-2	−0.73	0.09	12	4	This study
	−0.73	0.17	16	7	Nielsen et al. (2019)
	−0.70	0.10	37	n.g.	Wu et al. (2016)
	−0.50	0.19	4	4	Prytulak et al. (2011)
BIR-1	−0.92	0.12	17	5	This study
	−0.90	0.09	3	1	Qi et al. (2019)
	−0.89	0.23	3	2	Hopkins et al. (2019)
	−1.05	0.22	7	3	Sossi et al. (2018)
	−0.92	0.09	52	n.g.	Wu et al. (2016)
	−0.94	0.15	52	10	Prytulak et al. (2011)
SGR-1	−0.21	0.11	11	4	This study
SCO-1	−0.65	0.10	13	5	This study
SDO-1	−0.54	0.11	18	5	This study
BDH	−1.19	0.10	490		This study
	−1.24	0.08	367		Qi et al. (2019)
	−1.19	0.21	123		Hopkins et al. (2019)
	−1.13	0.12	28		Sossi et al. (2018)
	−1.22	0.08	10		Schuth et al. (2017)
	−1.23	0.08	197		Wu et al. (2016)
	−1.19	0.12	600		Nielsen et al. (2011)

n.g. – information not provided.
Analyses refer to the number of individual mass spectrometric analyses performed;
Splits refer to number of separate dissolved solutions of sample processed through the entire ion exchange column procedure.

Table 3
Leaching results of USGS shale reference materials.

	HNO_3 N	Temperature °C	$\delta^{51}V$ ‰	2SD	Analyses	Splits	Al wt.%	Ti µg/g	V µg/g
SDO-1									
Bulk digestion			−0.54	0.11	18	5	6.50	4260	160
HNO_3 Leaching	1	130	−0.48	0.08	3	1	1.00	25	35
	2	130	−0.47	0.10	6	1	1.27	46	45
	4	130	−0.55	0.07	3	1	1.79	85	61
	1.5	25	−0.49	0.11	3	1	0.31	18	9
	3	25	−0.44	0.08	9	3	0.37	34	11
	5	25	−0.50	0.10	3	1	0.39	45	12
SCO-1									
Bulk digestion			−0.65	0.10	13	5	7.25	3780	130
HNO_3 Leaching	1	130	−0.56	0.08	6	2	2.24	53	48
	2	130	−0.60	0.06	6	2	3.63	358	89
	4	130	−0.55	0.10	6	2	3.74	431	92
	1.5	25	−0.59	0.10	3	1	0.53	39	12
	3	25	−0.59	0.08	9	3	0.66	70	17
	5	25	−0.53	0.11	3	1	0.73	90	18

Analyses refer to the number of individual mass spectrometric analyses performed;
Splits refer to number of separate dissolved splits of sample processed through the entire ion exchange column procedure.

Table 4
Oxic global pelagic sediment sample data.

		VIN19 BC-27	CHN100 55PG	CHN100 57PG	CHN100 82PG	CHN100 85PG	CHN100 94PG	CHN100 96	All54 7PG	CHN13 PC-4	CHN39 2GCHP	CHN39 4GCHP
Latitude	°	51.23	16.55	18.03	7.19	7.21	10.08	7.51	8.49	53.53	25.18	27.55
Longitude	°	165.04	170.39	167.11	168.21	168.31	99.40	100.41	99.30	24.12	55.44	57.00
Water depth	m	5200	3316	4215	5742	5457	4314	4201	4375	3375	5937	5960
Sediment depth	cm bsf	0–2	0–4	0–4	0–4	0–3	0–10	0–4	0–4	5–7	0–3	0–3
Bulk data												
$\delta^{51}V$	‰	NA	NA	−0.76	NA	NA	−0.79	NA	−0.81	NA	NA	NA
2SD				0.08			0.02		0.12			
n				2			2		2			
TOC	wt.%	NA	NA	NA	NA	NA	NA	NA	NA	NA	NA	NA
Al	wt.%	7.47	7.89	7.42	6.89	4.62	2.30	1.66	1.52	5.80	9.54	9.38
Fe	wt.%	4.07	6.49	6.52	6.85	10.08	12.33	11.10	6.17	4.02	5.56	5.58
Mn	wt.%	0.24	0.17	0.22	0.73	8.98	3.36	3.13	2.18	0.13	0.53	0.69
Ti	μg/g	3548	4378	4245	9086	10,423	1252	893	818	5114	4805	4945
V	μg/g	147	252	219	158	273	176	160	108	115	162	158
Leaching data												
$\delta^{51}V$	‰	−0.87	−1.06	−0.71	−0.67	−1.14	−0.77	−1.07	−0.88	−0.79	−0.88	−0.77
2SD		0.10	0.13	0.12	0.01	0.08	0.06	0.08	0.11	0.07	0.05	0.01
n		2	2	2	3	2	3	2	3	3	2	3
Al	wt.%	0.53	0.35	0.46	0.40	0.71	0.15	0.23	0.21	0.36	0.83	0.50
Ti	μg/g	24	54	40	23	404	3	10	31	138	10	12
V	μg/g	15	16	42	26	134	102	109	65	16	41	34

		CHN75 25PG	CHN11538PC	CHN10031PG	CHN10046PG	All15763HC	AII9320PG	EPZTMC7	EPZT MC9	EPZT MC11	EPZT MC13	EPZT MC17
Latitude	°	12.59	34.04	3.13	1.26	32.01	2.01	12.00	12.00	12.00	14.00	15.00
Longitude	°	49.42	6.55	52.23	79.09	40.49	50.32	84.00	89.00	94.00	99.00	109.19
Water depth	m	1966	5260	5115	4475	4549	5080	4573	4149	3671	3859	3718
Sediment depth	cm bsf	3–6	0–2	0–4	0–4	0–3	0–4	0–1	0–1	0–1	0–1	0–1
Bulk data												
$\delta^{51}V$	‰	NA	NA	NA	NA	−0.97	NA	−0.82	−0.80	−0.85	−0.90	−0.95
2SD						0.07		0.05	0.07	0.13	0.03	0.06
n						2		3	2	2	2	2
TOC	wt.%	NA	NA	NA	NA	NA	NA	0.63	0.60	0.57	0.53	0.58
Al	wt.%	6.86	8.57	6.75	4.72	8.78	9.78	7.15	3.87	0.27	0.38	0.20
Fe	wt.%	3.54	5.17	4.32	2.84	5.06	5.26	4.29	3.28	0.26	0.76	0.35
Mn	wt.%	0.16	0.55	0.16	0.25	0.13	0.35	0.53	0.68	0.11	0.34	0.16
Ti	μg/g	3271	4543	4996	2428	5164	4982	5265	6810	1088	3404	1612
V	μg/g	107	116	108	71	106	111	165	94	5	12	5
Leaching data												
$\delta^{51}V$	‰	−0.88	−1.15	−1.10	−1.06	−0.85	−0.79	−0.73	−0.72	NA	−0.85	−0.98
2SD		0.06	0.02	0.08	0.02	0.08	0.05	0.03	0.11		0.01	0.05
n		2	2	2	2	2	2	2	2		2	2
Al	wt.%	0.55	0.27	0.44	0.30	0.36	0.34	0.77	0.72	NA	0.15	0.08
Ti	μg/g	19	3	13	17	11	8	126	171	NA	81	39
V	μg/g	31	15	17	13	17	15	31	22	NA	9	6

NA: not analyzed.

Table 5
Continental margin and euxinic basin sample data.

Sediment depth		Bulk data									Leaching data					
	cm bsf	$\delta^{51}V$	2SD	n	TOC wt.%	Al wt.%	Fe wt.%	Mn wt.%	Ti μg/g	V μg/g	$\delta^{51}V$	2SD	n	Al wt.%	Ti μg/g	V μg/g
Cape Basin (off Namibia)																
8449–1	4–5	NA			6.82	NA	NA	NA	NA	NA	−0.74	0.04	3	0.25	91	10
8451–1	4–5	NA			NA	NA	NA	NA	NA	NA	−0.80	0.06	3	0.21	66	9
8455–1	1–1.5	NA			NA	NA	NA	NA	NA	NA	−0.86	0.04	3	0.21	62	6
	2–3	NA			8.44	NA	NA	NA	NA	NA	−0.73	0.14	3	NA	NA	NA
8470–1	1–1.5	−0.87	0.14	3	NA	1.08	0.64	0.01	733	15	NA			NA	NA	NA
	3–4	−0.78	0.08	2	NA	1.14	0.66	0.01	733	15	NA			NA	NA	NA
Argentine Basin																
13813–1	5	NA			1.83	NA	NA	NA	NA	121	−1.15	0.09	2	0.45	86	18
	35	NA			1.72	NA	NA	NA	NA	124	−1.05	0.03	2	0.47	94	19
13809–2	5	−0.77	0.08	3	3.82	NA	NA	NA	NA	41	−0.86	0.01	2	0.49	154	16
	15	−0.75	0.06	3	3.77	NA	NA	NA	NA	43	−0.77	0.11	2	0.53	165	18
	25	NA			3.79	NA	NA	NA	NA	52	−0.82	0.18	2	0.45	142	15
13819–4	5	NA			0.79	NA	NA	NA	NA	115	−1.12	0.02	2	0.56	129	14
	35	NA			0.82	NA	NA	NA	NA	108	−1.11	0.01	2	0.66	149	15
Peruvian margin																
BIGO-05	5	−0.69	0.03	3	3.17	7.32	3.40	0.04	4600	140	−0.55	0.12	3	0.63	254	45
	10	−0.66	0.06	3	2.31	8.26	3.98	0.05	4800	135	−0.56	0.01	3	0.65	190	35
MUC29	5–6	−0.52	0.11	3	8.84	4.65	2.01	0.02	4300	156	−0.56	0.05	3	0.43	107	104
	8–10	−0.57	0.12	3	7.97	5.33	2.47	0.03	4600	122	−0.54	0.02	3	0.45	105	63
	12–14	−0.58	0.08	3	8.53	5.07	2.33	0.02	4600	122						
MW87/08 SC02	0–1	NA			NA	NA	NA	NA	NA	NA	−0.46	0.15	2	0.48	128	303
	40–41	NA			NA	NA	NA	NA	NA	NA	−0.46	0.01	2	0.52	167	63
MUC19	8–10	−0.53	0.10	3	16.17	3.90	1.42	0.02	3600	338	−0.55	0.04	3	0.47	122	245
	12–14	−0.47	0.08	6	14.04	3.72	1.37	0.02	3700	298	NA			NA	NA	NA
	14–18	NA			14.02	4.22	1.53	0.02	3600	223	−0.52	0.07	3	0.62	140	98
	30–34	NA			14.03	4.61	1.77	0.02	3800	149	−0.63	0.09	3	0.57	160	88
MUC33	6–8	−0.67	0.07	3	15.85	4.50	1.62	0.02	3600	155	−0.57	0.04	3	0.40	102	86
	10–14	−0.57	0.10	3	13.71	4.87	1.81	0.02	3700	146	NA			NA	NA	NA
	14–18	NA			11.55	4.89	1.84	0.02	3800	136	−0.57	0.11	3	0.57	157	68
	30–34	NA			3.34	7.11	3.47	0.04	4900	135	−0.52	0.08	5	0.67	258	53
MUC21	6–8	−0.53	0.09	2	3.53	7.42	3.04	0.03	4100	298	−0.28	0.07	3	0.78	178	74
	10–12	−0.43	0.12	3	7.84	6.88	3.07	0.03	4500	272	−0.26	0.11	3	0.81	269	151
	14–18	−0.36	0.00	2	7.85	7.64	2.76	0.03	3600	234	−0.13	0.09	3	0.70	222	145
MW87/08 SC06	0–1	NA			NA	NA	NA	NA	NA	NA	−0.63	0.06	2	0.57	189	87
	15–16	NA			NA	NA	NA	NA	NA	NA	−0.67	0.06	2	0.71	275	48
MUC25	6–8	−0.71	0.06	3	6.75	3.87	1.55	0.02	4000	64	−0.78	0.12	3	0.35	105	18
	10–12	−0.78	0.04	3	6.41	4.03	1.60	0.02	4000	68	−0.82	0.14	3	0.39	205	18
	14–18	NA			5.61	4.39	1.79	0.02	4100	70	−0.78	0.06	4	0.39	187	16
	22–26	NA			5.62	4.09	2.07	0.02	5100	79	−0.69	0.11	4	0.51	186	32
EPZT MC4	0–1	−0.81	0.01	2	4.59	5.20	2.76	0.03	2600	120	−0.72	0.05	2	0.32	85	20
MUC15	1–2	−0.91	0.06	3	4.60	4.14	2.33	0.02	5600	70	−0.94	0.10	5	0.40	116	17
	4–5	−0.90	0.03	3	3.87	4.29	2.75	0.02	6400	81	−1.05	0.13	3	0.44	98	17
	6–8	NA			4.11	4.42	3.70	0.02	8400	79	−0.95	0.08	3	0.43	107	17
	10–12	NA			4.27	4.35	4.22	0.02	9700	84	−0.94	0.08	2	0.41	99	15
MUC53	1–2	−0.82	0.07	2	4.00	4.22	2.26	0.02	5400	70	−1.04	0.05	3	0.42	97	14
	6–8	NA			3.33	4.54	3.00	0.02	6600	69	−0.90	0.11	3	0.43	111	14
MUC26	1–2	−0.82	0.03	2	2.94	5.02	2.47	0.03	4900	66	−0.78	0.05	3	0.38	103	13
	5–6	NA			3.04	5.07	2.48	0.03	4900	68	−0.99	0.01	2	0.37	148	12
	14–15	NA			2.70	4.96	2.45	0.03	4900	68	−0.85	0.09	2	0.39	156	11
MUC27	2–3	−0.71	0.07	2	4.24	5.87	2.36	0.03	4000	84	−0.84	0.06	3	0.52	137	19
	6–7	NA			2.71	6.11	2.27	0.04	3700	82	−0.82	0.01	2	0.37	148	12
	13–14	NA			1.64	5.85	2.22	0.04	3800	82	−0.72	0.01	2	0.39	156	11
Santa Barbara Basin																
NH01 G6C-47	0–1	−0.55	0.07	2	NA	8.59	4.51	0.03	4053	150	−0.37	0.08	2	0.61	255	70
	1–2	NA			NA	8.77	4.54	0.03	4100	151	−0.37	0.01	3	0.58	258	63
	2–3	NA			NA	9.50	4.77	0.04	4499	150	−0.40	0.05	2	0.57	274	55
	10–11	NA			NA	8.74	4.62	0.03	4132	150	−0.43	0.01	2	0.56	266	60

Table 5 (*continued*)

Sediment depth	cm bsf	Bulk data δ51V	2SD	n	TOC wt.%	Al wt.%	Fe wt.%	Mn wt.%	Ti μg/g	V μg/g	Leaching data δ51V	2SD	n	Al wt.%	Ti μg/g	V μg/g
Cariaco Basin																
PL07-22BX	0–1	NA			NA	NA	2.68	NA	2418	192	−0.22	0.12	3	0.27	28	56
PL07-89BX	0–1	NA			NA	NA	4.27	NA	3412	260	−0.28	0.08	3	0.36	38	67
PL07-82BX	0–1	NA			NA	NA	3.35	NA	2966	226	−0.26	0.04	3	0.35	35	65
PL07-105BX	0–1	NA			NA	NA	4.25	NA	3307	266	−0.25	0.09	3	0.34	40	74
PL07-67BX	0–1	NA			NA	NA	3.53	NA	3282	282	−0.13	0.06	3	0.33	25	73
PL07-69BX	0–1	NA			NA	NA	3.92	NA	3648	265	−0.27	0.05	4	0.37	44	64
PL07-111BX	0–1	NA			NA	NA	4.36	NA	3975	293	−0.13	0.05	4	0.40	49	76

NA: not analyzed.

3.2. V isotopic measurement

The purification of V was conducted with a four-step ion-exchange procedure by coupling cation-and anion-exchange columns after Wu et al. (2016), with minor modifications as described in Nielsen et al. (2019). Briefly, samples were first loaded on a cation resin AG50W-X12 (200–400 mesh) and major cations Al, Ti, and Na were eluted with 0.8 N HNO_3 + 0.1 N HF and 0.8 N HNO_3. V was then eluted and collected with 1.2 N HNO_3. The major cations Fe, Mg and Ca do not leave the resin by the time all of the V is eluted, thus the procedure separates all major cations except for K. The anion exchange resin AG1-X8 (200–400 mesh) was subsequently applied to remove all the residual matrix elements from V as described in Nielsen et al. (2011). The anion column was performed twice in order to quantitatively remove any residual Ti and Cr. In-between each column, samples were evaporated and refluxed in aqua regia overnight at 135℃ to remove potential organic material leached from the resin, evaporated again, and re-dissolved in the next solution. The yield of the entire V column chemistry procedure is within error of 100% (Wu et al., 2016). Samples were re-dissolved in 1 mL 2% HNO_3 prior to elemental and isotopic analysis. Total procedural blanks (from sample dissolution/leach to instrumental analysis) were < 2 ng, which is negligible compared with the amount of V extracted from each sample (2–6 μg).

In this study, V isotope analysis of all samples were conducted using the a Thermo Neptune MC-ICPMS at Florida State University (FSU) within the geochemistry group at the National High Magnetic Field Laboratory. Measurements were performed on the flat-topped shoulder on the lower mass side of the overlapping V and molecular interference peaks in medium-resolution mode (resolution ΔM/M > 4000) to resolve all interfering molecular species representing combinations of C, N, O, S, Ar and Cl (such as $^{36}Ar^{14}N^+$, $^{36}Ar^{16}O^+$, and $^{38}Ar^{14}N^+$, see Nielsen et al., 2016; Wu et al., 2016). To obtain the highest possible V transmission efficiency, solutions were introduced with a desolvating nebulizer system (Aridus II) and Jet sample and Ni X-skimmer cones were also applied. The typical sensitivity of ^{51}V under such configuration was ~1.5–2.5 nA/ppm.

Sample analysis protocols follow standard-sample bracketing procedures as described previously (Nielsen et al., 2011; Wu et al., 2016). The 10^{10} Ω resistor is applied to monitor ^{51}V, while other concerned isotopes (^{49}Ti, ^{50}V, ^{52}Cr, ^{53}Cr) are monitored with conventional 10^{11}Ω resistors to accommodate the large natural isotope abundance differences of V ($^{51}V/^{50}V$ = ~400). While the chemical purification nearly quantitatively separates Ti and Cr from V, minor amounts of ^{50}Ti and ^{50}Cr remain in solution which can dramatically affect the analysis on $^{51}V/^{50}V$ ratio, especially for low V concentration measurements. Therefore, analysis of the $^{49}Ti/^{51}V$ and $^{53}Cr/^{51}V$ ratios are needed and should be less than 0.00005 to properly correct for interferences of ^{50}Cr and ^{50}Ti. Here we use the procedure described by Nielsen et al. (2011) and Wu et al. (2016) to correct the raw data for any potential interferences. Briefly, 50 ng/g Cr and 50 ng/g Ti standard solutions were analyzed every time the mass spectrometer was re-tuned to calculate the mass bias coefficients. The obtained mass bias coefficients were then used to calculate the true ^{50}Ti and ^{50}Cr ion beam that was subtracted from the total signal on mass 50.

All V isotope measurements from different labs mentioned in this study used the aliquots of the Alfa Aesar (AA) V standard made and distributed by Nielsen et al. (2011) and Prytulak et al. (2011) as the bracketing solution. Vanadium isotopic data are reported in conventional δ-notation in permil relative to AA ($\delta^{51}V$ (‰) = 1000 × [($^{51}V/^{50}V_{sample}$ − $^{51}V/^{50}V_{AA}$)/$^{51}V/^{50}V_{AA}$]). Each data analysis was run with 40 cycles of 4.194 s integrations for each cycle and baseline calibration was run before each analysis. Each sample was bracketed by measurements of the AA solution to obtain an average value and stability of the instrument for the highest quality control. After the evaluation of two samples, a solution standard, BDH, was measured to ensure the performance and stability of the analysis on the MC-ICP-MS. The in-house isotope BDH standard was a 1000 μg/g V standard solution originally bought from BDH Chemicals (Nielsen et al., 2011), which has an isotope composition of $\delta^{51}V = -1.2$‰ based on analyses in several different labs worldwide (Table 2). The errors for V isotope results of each sample are reported in two standard deviations relative to the average value (2SD). Measurements of BDH in this study gave an average $\delta^{51}V = -1.19 \pm 0.10$‰ (2SD, n = 121). The USGS igneous rocks reference materials BCR-2, BIR-1, and AGV-2 were processed through the same ion-exchange procedures and $\delta^{51}V$ values are in agreement with literature values, as shown in Table 2. In addition, three USGS organic shale reference materials SGR-1, SCo-1, and SDO-1 were analyzed and are pre-

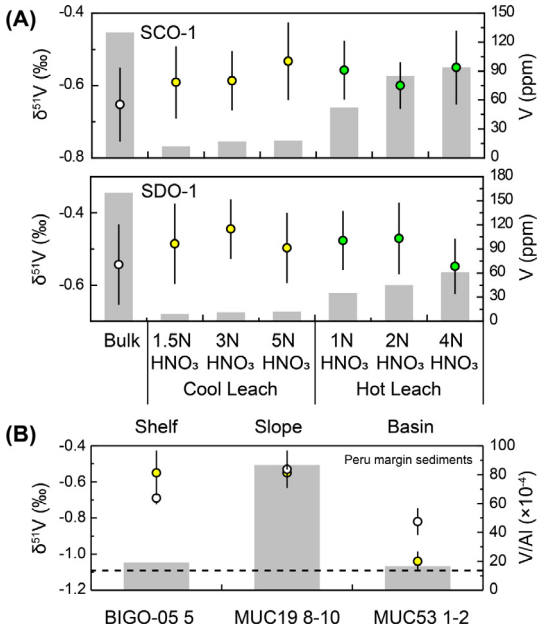

Fig. 2. Vanadium isotope results from various digestion methods. (A) white dot refers to the $\delta^{51}V$ of bulk digestion, green dot refers to the $\delta^{51}V$ of leaching proportion with various HNO_3 strengths under 130℃, and yellow dot refers to the $\delta^{51}V$ of leaching proportion with various HNO_3 strengths under room temperature (~25 °C). The V contents for the bulk digestion and leaching proportion are also shown with grey bars. (B) Bulk and leaching V isotope compositions of selected modern Peruvian margin samples with the bulk V/Al ratio of each sample. White dot refers to the $\delta^{51}V$ of bulk digestion, and yellow dot refers to the $\delta^{51}V$ of leaching proportion with 3 N HNO_3 strengths under room temperature (~25 °C). The bulk V/Al ratio is showed with grey bars. Dashed lines depict the reference lithogenic background on the Peruvian continental margin sediments (Scholz et al., 2011). (For interpretation of the references to colour in this figure legend, the reader is referred to the web version of this article.)

sented in this study for the first time. The uncertainties of $\delta^{51}V$ for reference materials are better than ± 0.12‰ (2SD), representing the long-term external reproducibility of the data in this study.

4. RESULTS

Elemental abundances of Al, Ti, and V, and $\delta^{51}V$ data for leached and/or bulk results of all samples are presented in Tables 3–5 and have been plotted in subsequent figures.

4.1. Leaching results of the shale standards

In general, the elemental abundances increase with increasing HNO_3 strength and reactive temperature, which indicates that more material is being dissolved (Table 3 and Fig. 2). However, the leaching fractions with various HNO_3 strengths and reactive temperatures document a homogeneous V isotope composition. Therein, SCo-1 samples have a mean $\delta^{51}V_{leach}$ value of −0.57 ± 0.05‰ (2SD, n = 11), and SDO-1 have mean $\delta^{51}V_{leach}$ value of −0.49 ± 0.07‰ (2SD, n = 8) for all leaching methods.

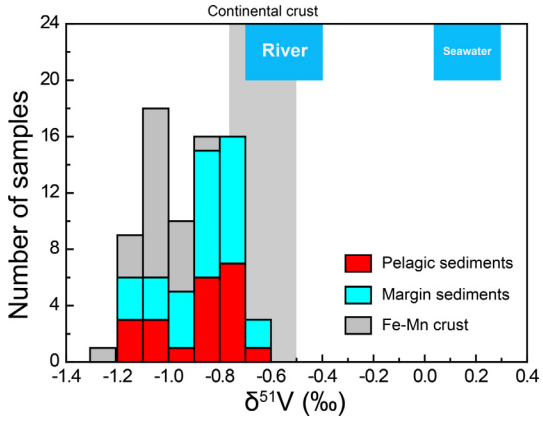

Fig. 3. Histogram of the V isotope values measured in Pelagic sediments and continental margin sediments deposited under seawater with bottom oxygen content > 10 μM. Also shown are the histogram of the V isotope values measured in hydrogenetic Fe-Mn crust (Wu et al., 2019b), and the likely ranges of V isotope composition of continental crust (Wu et al., 2016), river (Schuth et al., 2019), and seawater (Wu et al., 2019a).

4.2. Pelagic sediments

The V isotope composition for the leachable fraction of these globally distributed oxic sediments ranges from −1.15‰ to −0.67‰ (Fig. 3), with a mean value of −0.89 ± 0.30‰ (2SD, n = 21). These samples have large V variations from 5 μg/g to 275 μg/g, with V/Al ratios ranging from 11.4 to 96.7 × 10^{-4}, of which the lower end is close to the average upper continental crust (11.9 × 10^{-4}; Rudnick and Gao, 2003) and the upper values suggesting a nearly tenfold V enrichment compared to Al. The V/Al ratios of pelagic sediments show a strong positive correlation to Fe/Al ratios ($R^2 = 0.92$), while no correlation to the $\delta^{51}V_{leach}$ ($R^2 = 0.04$) is observed. The $\delta^{51}V$ values measured on the selected samples with bulk digestion are analytically indistinguishable from the corresponding leachable $\delta^{51}V$ values as shown in Table 4.

4.3. Continental margin sediments

4.3.1. Argentine basin and cape basin

All the sediments from the continental margin along the Argentine Basin and Cape Basin were collected from stations with oxic bottom water conditions where O_2 contents were higher than 100 μM. Overall, these samples have $\delta^{51}V_{leach}$ values ranging from −0.73‰ to −1.15‰ (Fig. 3). Therein, the oxic samples from four stations in Cape Basin show a relatively narrow range of $\delta^{51}V$ with an average value of −0.80‰ ± 0.11‰ (2SD, n = 6). For sediments from the Argentine Basin, samples from station 13809–4 have an average value of $\delta^{51}V_{leach} = -0.81 \pm 0.09$‰ (2SD, n = 3), while samples from station 13813–1 and 13819–4 have indistinguishable values of $\delta^{51}V_{leach} = -1.10 \pm 0.08$‰ (2SD, n = 4).

4.3.2. Peruvian margin

The sampling stations from the Peruvian margin area around 11°S are ordered according to increasing water

depth and classified into four zones related to bottom water redox conditions and pore water profiles (for detailed information see Scholz et al., 2011). For simplicity, these schemes are used to document the redox transect from the shallowest anoxic Zones I and II without detectable dissolved oxygen in the bottom water ($O_2 < 1.5$ μM), to Zone III with trace dissolved oxygen in bottom water ($O_2 <$ ~10 μM), and to the deepest and least reducing Zone IV ($O_2 >$ ~10 μM).

The Peruvian margin sediments have $\delta^{51}V_{leach}$ values ranging from −0.13‰ to −1.05‰ (Table 5). Despite the large overall V isotope range, down core samples collected from each station show relatively homogenous V isotope composition for each core. In addition, the stations in different zones show different ranges of sedimentary $\delta^{51}V_{leach}$ values. Therein, the sediments from stations within Zones I and II have very limited ranges of leachable V isotope compositions with an average $\delta^{51}V_{leach} = -0.54 \pm 0.10$‰ (2SD, n = 12). The samples collected from two stations within Zone III have a large range of $\delta^{51}V_{leach}$ values, with MUC21 (water depth of 465 m, bottom water O_2 content of 2.1 μM) samples having an average $\delta^{51}V_{leach} = -0.22 \pm 0.16$‰ (2SD, n = 3) while MW87/08 SC02 (water depth of 535 m, bottom water O_2 content of ~ 9 μM) samples have an average $\delta^{51}V_{leach} = -0.65 \pm 0.05$‰ (2SD, n = 2). Note that the station MW87/08 SC02 is collected from ~15°S, thus might not be directly compared to other sampling stations from 11°S. For comparison, the $\delta^{51}V_{leach}$ of samples from stations in Zone IV varied from −0.69 to −1.05‰, significantly lower than those of samples from stations in Zone I, II and III. A select number of samples were also analyzed for the bulk digestion and V isotope analysis. The $\delta^{51}V$ values range from −0.36‰ to −0.91‰ in the bulk sediment of these samples.

4.3.3. Santa barbara basin

$\delta^{51}V$ data for the deep basin core samples from Santa Barbara Basin are presented in Table 5. The V isotope composition for the leachable fraction of these samples document a limited range with an average of -0.39 ± 0.06‰ (2SD, n = 4). The bulk $\delta^{51}V$ value of the core-top sediment (0–1 cm) is −0.55‰, a little lighter than the corresponding leachable $\delta^{51}V$ values (−0.37‰).

4.4. The euxinic Cariaco Basin

$\delta^{51}V$ data for the Cariaco Basin samples are presented in Table 5. These samples are core-top sediments from sites with water depths from 400 to 1400 m, all located below the chemocline. The leachable fraction of these core-top samples shows limited V isotope variations with an average of $\delta^{51}V_{leach}$ value of -0.22 ± 0.12‰ (2SD, n = 7), despite that they are widely distributed across the Cariaco Basin and collected from both sub-basins.

5. TESTING THE VALIDITY OF THE LEACHING METHOD

To track ocean redox conditions it is required to analyze the authigenic V fraction as it is directly extracted from seawater. Therefore, a method is required that can isolate the authigenic V isotope composition from the detrital fraction because bulk dissolution captures a mixture of both fractions. The detrital V concentrations are significant compared to authigenic enrichments in some sediments, and bulk V isotope analyses of such sediments might result in obtaining a non-authigenic V isotopic signature (e.g. Böning et al., 2004). For instance, the lithogenic V fractions of the sediments from the Peruvian Margin in this study have been estimated by normalizing the sedimentary V content to the insoluble detrital tracer Al, and by comparing their V/Al ratios to that of the average Andesite in the Andean Arc, which is suggested to be an appropriate representation of the detrital background for the Peruvian margin (Scholz et al., 2011). The results showed that even the lithogenic V fractions of sediments deposited within the OMZ are significant, although generally lower than that of oxic sediments. Thus, it is essential to isolate the authigenic component from the bulk sediment. In this study, a sequential extraction method was developed based on previous studies for Cr isotopes (Reinhard et al., 2014) and tested to isolate the authigenic V isotope signature from detrital V.

The leaching results of shale SRM SCo-1 and SDO-1 show that variable acid strengths and different reaction temperatures affect the absolute amount of V that is mobilized from the host sediment (Fig. 2a). However, the V isotopic composition of all leachates for these sediments are analytically indistinguishable. The lack of any notable effect of acid strength and reaction temperature on measured leachate V isotope composition suggests that (1) the leachable V in shales is hosted within an isotopically homogeneous pool, and (2) the leachable V is mobilized congruently (albeit sometimes non-quantitatively) without any isotope fractionation during the leaching process. Thus, it is likely that the isotope composition of the leachable V with dilute HNO_3 represents the isotope composition of the authigenic V pool in marine organic-rich siliciclastic sediments. For the studied organic-rich sediments, we apply the 'cool leach' method with 3 N HNO_3 to avoid the potential extraction of the lithogenic phase, since the 'cool leach' method generally is conservative with respect to the lowest percentage of Al extracted from the sediments (<10% of Al in total sediments, Table 3) and has an analytically indistinguishable isotope value.

To further test the reliability of this leach method, the leach and bulk V isotope compositions of three representative samples from the Peruvian margin depth transect are also presented in Fig. 2b. These samples have various V/Al ratios and thus different contributions of lithogenic V input. For example, the sample MUC19 8–10 cm has an elevated V/Al ratio (86.7×10^{-4}) compared to the lithogenic background (13.9×10^{-4}, Scholz et al., 2011) due to an authigenic enrichment, and the V isotope composition of the leachable V fraction (-0.53 ± 0.04‰) is analytically indistinguishable from its bulk value (-0.53 ± 0.10‰). This result is as expected given that the majority of V in this sediment (~85%) is likely due to authigenic enrichment from seawater. Therefore, the V isotope composition of bulk sediment should be very close to the authigenic value. For

comparison, the V isotope composition of the leachable V is distinctly different to the bulk value for the sediments (BIGO-05 5 cm and MUC53 1–2 cm) with V/Al ratios (16.6×10^{-4} and 19.1×10^{-4}, respectively) that are only slightly enriched compared to the assumed lithogenic background (13.9×10^{-4}, Scholz et al., 2011). For these two samples $\delta^{51}V_{leach}$ were highly disparate (−0.55‰ and −1.04‰, respectively) whereas their $\delta^{51}V_{bulk}$ values are only different by 0.13‰. If we use the V/Al ratios in the bulk sediment and the assumed lithogenic background to calculate the relative contributions of authigenic and lithogenic V, we can use the measured $\delta^{51}V_{leach}$ and $\delta^{51}V_{bulk}$ to calculate that the lithogenic component in both samples exhibit indistinguishable $\delta^{51}V$ around −0.75‰ (−0.74‰ for BIGO-05 5 cm and −0.78‰ for MUC53 1–2 cm). This lithogenic value is similar to published V isotope data for andesites that show $\delta^{51}V$ from −0.80‰ to −0.65‰ (Wu et al., 2016, 2018; Prytulak et al., 2017). This observation is consistent with previous studies that found the detrital flux to the Peruvian margin is likely dominated by andesite-like material (Böning et al., 2004; Scholz et al., 2011). These results provide additional evidence that our leaching method extracts only authigenic V from modern marine organic-rich siliciclastic sediments. Additionally, our data document the significance of applying a leaching technique to samples that contain low V enrichments or are dominated by high lithogenic V.

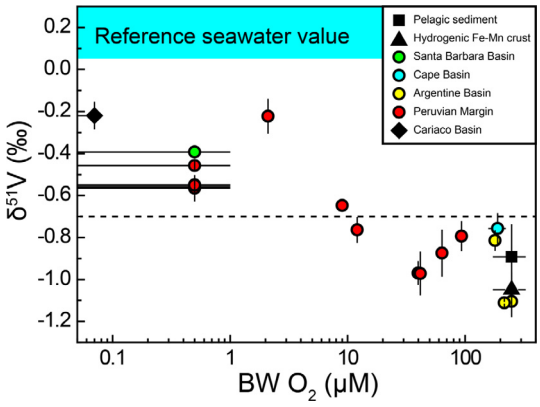

Fig. 4. Vanadium isotope composition of marine sediments with various bottom water O_2 contents. The colored dots represent the average authigenic $\delta^{51}V$ values of the continental margin sediments for each station with at least two samples. The black diamond represents the average authigenic $\delta^{51}V$ values for the euxinic core-top sediments from Cariaco Basin. The black square represents the average authigenic $\delta^{51}V$ values for pelagic sediments in this study. The black triangle represents the average $\delta^{51}V$ values for hydrogenic Fe-Mn crust from Wu et al. (2019b). Note that the sample stations from Peruvian margin OMZ and deepest Sabra Barbara Basin are under seawater with absence of both detectable amounts of oxygen and H_2S. Sediments under sulfidic seawater in Cariaco Basin are under seawater characterized by zero dissolved oxygen and with present of H_2S. To show the variations of $\delta^{51}V$ with bottom oxygen more clearly, we use log scale for the bottom oxygen contents, and denote the BW O_2 of those OMZ sediments and euxinic sediments with ~ 0.5 μM and < 0.1 μM, respectively. Dashed lines give a reference boundary for the authigenic $\delta^{51}V$ of samples deposited under oxygen deficient bottom water and less reducing environments with bottom water O_2 > 10 μM. The error bar represents one standard deviation.

6. DISCUSSION

6.1. Redox controls the V isotope variations in marine sediments

The empirical relationship between sedimentary $\delta^{51}V_{leach}$ values and bottom water oxygen concentrations is shown in Fig. 4. Modern sediments underlying oxygen-deficient bottom waters (BW O_2 < ~10 μM) all have $\delta^{51}V > -0.7$‰, which is markedly different from that of sediments deposited under oxic bottom water conditions with contents > ~10 μM that exhibit $\delta^{51}V$ values ranging from −1.1 to −0.7‰. In addition, the Cariaco Basin core-top sediments collected under anoxic and sulfidic bottom water have the most positive V isotope compositions among all the studied sediments (Fig. 4). Thus, V isotope variation in marine sediments indicates a strong relation-

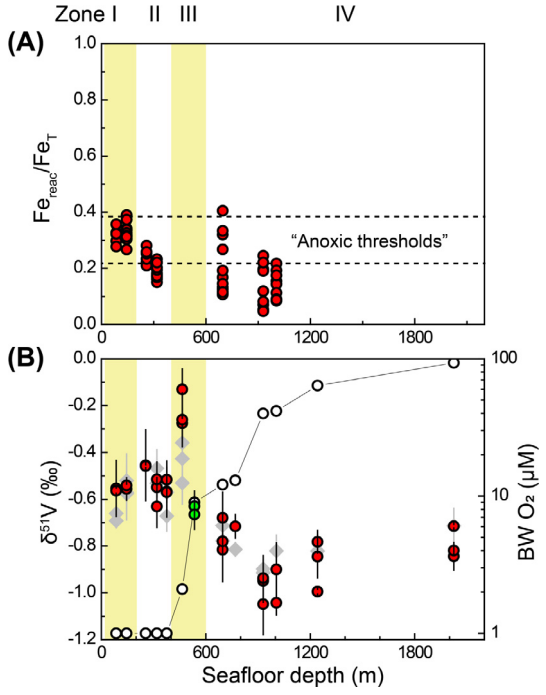

Fig. 5. (A) Lateral distribution with deposition depth of sedimentary V isotope and Fe species across the Peruvian continental margin. The four zones are classified by Scholz et al (2011) based on the shape of the pore water profiles of the sediment cores at ~11°S. Fe_{HR}/Fe_T data is from Scholz et al. (2014a). Dashed lines in (A) depict the suggested boundaries between oxic ($Fe_{HR}/Fe_T \leq 0.22$) and anoxic ($Fe_{HR}/Fe_T \geq 0.38$) depositional conditions based on iron speciation (Poulton and Canfield, 2011). (B) $\delta^{51}V$ of Peruvian continental margin sediments. $\delta^{51}V$ values of the bulk samples are shown with grey diamonds; $\delta^{51}V$ values of the leach proportion are shown with colored dots. Note that the green dots show data of sediments collected from ~15°S, thus might not be directly compared to other sediments (data shown as red dots) from 11°S. The BW O_2 (bottom seawater oxygen content) of each sampling station is shown by blank dots.

ship between the authigenic V isotope composition and environmental redox conditions overlying the sediments.

Further evidence for the redox related sedimentary V isotope composition is observed in $\delta^{51}V$ variations in the Peruvian Margin sediments. For the Peruvian Margin transect from the reducing OMZ to the oxic seafloor, the spatial $\delta^{51}V$ variability is shown in Fig. 5 with bottom water oxygen contents. The change in authigenic V isotope composition is observed within the Peruvian margin sediments from around −0.5‰ in the reducing Zone I and Zone II to up to −1.1‰ in the oxic Zone IV, and this isotopic shift most clearly documents the relationship between V isotopes and changes in the bottom water oxygen contents between 0 and > 10 μM O_2 (Fig. 5). It is also noteworthy that different sediment localities in the Peruvian margin OMZ transect document large variations in sedimentation rates (Scholz et al., 2011). The samples from shallow stations close to the continental margin have sedimentation rates up to about 160 cm kyr^{-1}. For comparison, the samples from more offshore stations have sedimentation rates as low as ~30 cm kyr^{-1} (Scholz et al., 2011). Sediments in the anoxic zones termed I and II also show large V/Al variations from 17×10^{-4}, similar to that in Zone IV, which is very close to detrital background (~14×10^{-4}, Scholz et al., 2011), to ratios up to 90×10^{-4} (Fig. 6). However, the authigenic V isotope compositions show limited range and analytically indistinguishable for these sediments in anoxic Zones I and II (all around −0.5‰, Figs. 5 and 6).

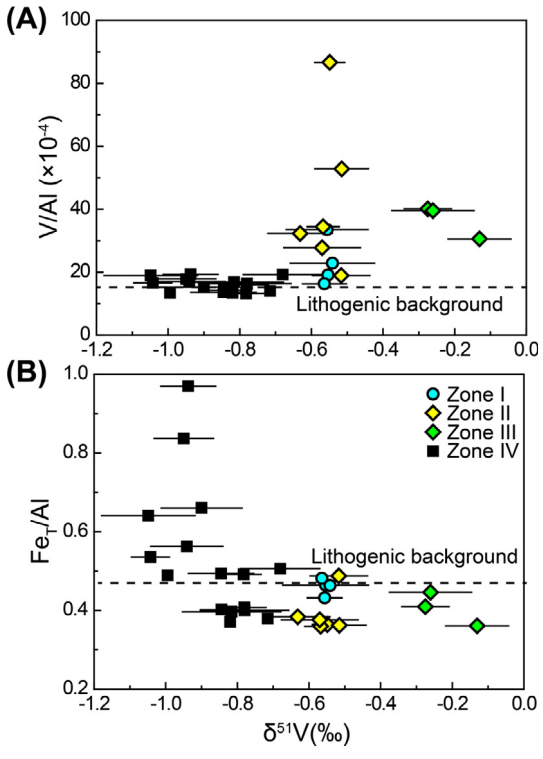

Fig. 6. Authigenic V isotope composition ($\delta^{51}V_{leach}$) versus (A) bulk V/Al ratios and (B) bulk Fe_T/Al ratios in the studied Peruvian continental margin sediments. Dashed lines in (A) and (B) depict the reference lithogenic background on the Peruvian continental margin sediments (Scholz et al., 2011).

This observation suggests that the isotopic composition of the authigenic V is not strongly influenced by their local sedimentation rate. The same is also observed for the sediments in the Santa Barbara Basin where $\delta^{51}V_{leach} \sim -0.4$‰ (Table 5), which is close to that of central OMZ Peruvian margin sediments, despite its high sedimentation rates of about 100–200 cm kyr^{-1} (Reimers et al., 1990; Zheng et al., 2000), and muted V enrichment with V/Al ratios of around 17×10^{-4}. For comparison, the continental margin sediments deposited under oxic bottom waters exhibit a range in $\delta^{51}V_{leach}$ that is remarkably similar to that found for abyssal pelagic clays, despite their variable but high TOC contents (Fig. 3). Thus, we propose that the authigenic sedimentary V isotope signatures are dominantly controlled by the local bottom water redox state rather than other factors like organic carbon burial, sedimentation rate, or total V enrichment.

To fully evaluate the V isotope proxy it is useful to make a comparison to Fe speciation, as it is one of the most widely utilized geochemical tools to assess local redox conditions in ancient marine environments (e.g. Raiswell et al., 1988; Canfield et al., 1992; Raiswell and Canfield, 1998; Poulton and Canfield, 2011; Raiswell et al., 2018). Iron speciation has been used to distinguish oxic, ferruginous (anoxic and iron-rich), and euxinic (anoxic and H_2S-containing) environments. The Fe_{HR}/Fe_T has also been evaluated for a subset of the Peruvian margin samples studied here (Scholz et al., 2014b), as shown in Fig. 5. Although there is a general trend of decreasing Fe_{HR}/Fe_T ratios from shelf to deep slope, none of the Fe_{HR}/Fe_T ratios are above the unambiguous oxic-anoxic threshold ratio of 0.38 (Poulton and Canfield, 2011). It is known that the extent of reactive Fe enrichment also strongly depends on background sedimentation, which is comparably high in the offshore Peruvian margin (Scholz, 2018). Some Peruvian margin sediments underneath oxygen-deficient bottom waters are even depleted in highly reactive iron (with muted Fe_{HR}/Fe_T ratio), that might be the result of remobilization and transport of Fe_{HR} under low oxygen but non-euxinic conditions (Scholz et al., 2014a, 2014b). For comparison, the vanadium isotope signature of these sediments appears to record the depositional redox transition from essentially anoxic through to oxic environments. Hence, using $\delta^{51}V_{leach}$ values as a redox proxy for local conditions that are less affected by other factors like the background sedimentation rates has the potential to provide additional and probably more nuanced constraints on reconstructing ancient bottom water oxygen fluctuations at the oxygen deficient range.

6.2. Mechanisms controlling isotope fractionation of authigenic V in marine sediments

The data presented here suggest that the authigenic sedimentary V isotope composition is strongly controlled by the local bottom water redox conditions. However, the exact mechanisms that govern such a relationship remain uncertain. To address this uncertainty we will discuss the potential controls on the V isotope fractionation during the formation of authigenic V components in marine sedi-

ments. This will provide a framework for interpreting the redox related authigenic V isotope variations in marine sediments based on currently available data.

6.2.1. Oxic sediments

The typical V content in average pelagic sediments is ~117 μg/g (Bischoff et al., 1979), but the concentration of V can vary dramatically in pelagic sediments (2–955 μg/g, South Pacific pelagic clay, Dunlea et al., 2015). The enrichment of authigenic V in pelagic sediments has been ascribed to the accumulation of V associated with Fe-Mn (oxyhydr) oxide minerals that precipitate from the water column (e.g. Dunlea et al., 2015). An experimental study by Koschinsky et al. (2003) also shows that Fe-Mn oxides and oxyhydroxides are the most important phases, compared to other seawater particles like clay minerals, in scavenging many dissolved metals from seawater including V. Such a conclusion is also supported by our data, which show a positive correlation between V/Al ratios and Fe/Al ratios of studied pelagic sediments ($R^2 = 0.92$). A recent study suggests that pure marine hydrogenetic Fe-Mn crusts and nodules have a relatively homogeneous V isotope composition ($\delta^{51}V = -1.05 \pm 0.16‰$; Wu et al., 2019b), which corresponds to fractionation from seawater ($\delta^{51}V = 0.20 \pm 0.15‰$; Wu et al., 2019a) of $\Delta_{FeMn\text{-}sw} = -1.25 \pm 0.22‰$. The isotope fractionation has been explained by the adsorption of pentavalent vanadate onto Fe-Mn oxyhydroxides (Wu et al., 2015; 2019b). The average V isotope composition for the authigenic fraction of pelagic sediments is $\delta^{51}V = -0.89 \pm 0.30‰$ (2SD, $n = 21$), which corresponds to a fractionation factor of $\Delta_{PelClay\text{-}sw} = -1.09 \pm 0.33‰$ that is within the error of the value obtained for hydrogenetic Fe-Mn deposits. In addition, the varible enrichment extents of V, indicated by $V/Al = 11.4$ to 96.7×10^{-4}, shows no correlation to the $\delta^{51}V_{leach}$ variations ($R^2 = 0.04$). Thus, the isotope composition of authigenic V in the oxic pelagic sediments is proposed to be controlled by the isotope fractionation of V during its accumulation with Fe-Mn oxyhydroxide sediment components.

Another process that could affect V isotope compositions recorded in oxic sediments is remobilization of V within the porewaters of marine sediment deposited under oxic bottom waters where organic matter remineralization causes rapid oxygen depletion below the sediment–water interface (e.g. Morford and Emerson, 1999; Morford et al., 2005; Scholz et al., 2011). These processes have been suggested to potentially cause V depletions when sediment porewaters are released back into the water column due to diffusion and sediment compaction (Morford and Emerson, 1999). Despite the variable but high TOC contents and very small oxygen penetration depth (<3cm) that induces redox cycling of V within the sediment porewaters, the studied oxic continental margin sediments show a range of $\delta^{51}V_{leach}$ values remarkably similar to that found for abyssal pelagic clays (Fig. 3). In addition, these oxic sediments show distinct V isotope compositions compared to the sediments deposited under oxygen-deficient seawater (Figs. 4 and 5). These observations suggest that the authigenic V is also accumulated into continental margin oxic sediments with Fe-Mn oxyhydroxide, and processes that redistribute and/or deplete V within these types of sediments do not modify the primary V isotope signature.

It is notable that the $\delta^{51}V$ of oxic sediments (pelagic and continental margin sediments) are more variable and generally exhibit more positive values than pure hydrogenetic Fe-Mn deposits (Fig. 3). This might imply that not all the authigenic V is associate with the Fe-Mn oxyhydroxides. Previous studies suggest that authigenic clay and/or phosphate phases might also incorporate some V from oxic seawater (Collier, 1984; Wehrli and Stumm, 1989), although it is much less efficient compared to the Fe-Mn (oxyhydr)oxides (Koschinsky et al., 2003). However, no correlation between Fe/Al and $\delta^{51}V$ of oxic sediments is observed, thus there is no evidence that conclusively supports the influence on authigenic V isotope compositions from other authigenic phases. Also, since we have no constraints on the V isotope composition of authigenic clay minerals or phosphate phases, it is difficult to quantify whether the V isotope variations observed are related to these phases or variations in the V isotope fractionation factor between Fe-Mn (oxyhydr)oxides and seawater.

6.2.2. Continental margin oxygen-deficient sediments

The changes in authigenic V isotope composition for marine sediments deposited in open ocean seawater, but with different local redox conditions, must be controlled by changes in isotope fractionation during the delivery and/or burial of V into marine sediments from seawater. Sedimentary enrichments of V under reducing seawater are known to relate to the reduction of dissolved pentavalent vanadate to reduced V species that are prone to removal from the dissolved phase (e.g. Breit and Wanty, 1991). The delivery of reduced redox-sensitive metals, like V, in reducing sediment could be described in two endmember pathways: delivery and accumulation through metal diffusion across the sediment–water interface and/or delivery to the surface sediments by marine particulate matter in the oxygen-deficient water column (e.g. Zheng et al., 2002; Scholz et al., 2017). For the diffusive delivery pathway, the continuous removal of the element within the pore fluids below the sediment–water interface results in a decreasing abundance, with a gradient from overlying bottom waters to the pore fluids metal removal (Fig. 7). Conversely, the authegenic metals delivered by settled particulates generally are controlled by various extents of redissolution that release metals into pore fluids and results in peak enrichments within the pore fluids at or near the sediment–water interface (Fig. 7).

The pore water profiles of several redox-sensitive metals including V in our studied Peruvian margin sediments have been analyzed and reported in Scholz et al. (2011), which can provide some evidence for the likely supply pathway of V in these sediments. With the exception of a few stations in Zone III, no V depletion in the pore waters close to the sediment–water interface compared to seawater is observed (Fig. 7). This observation suggests that the diffusional supply of V to sediments within oxygen-deficient bottom waters is not likely to be the dominant means of V enrichment. On the other hand, the pore water profiles generally show fluctuations of V around the seawater values and

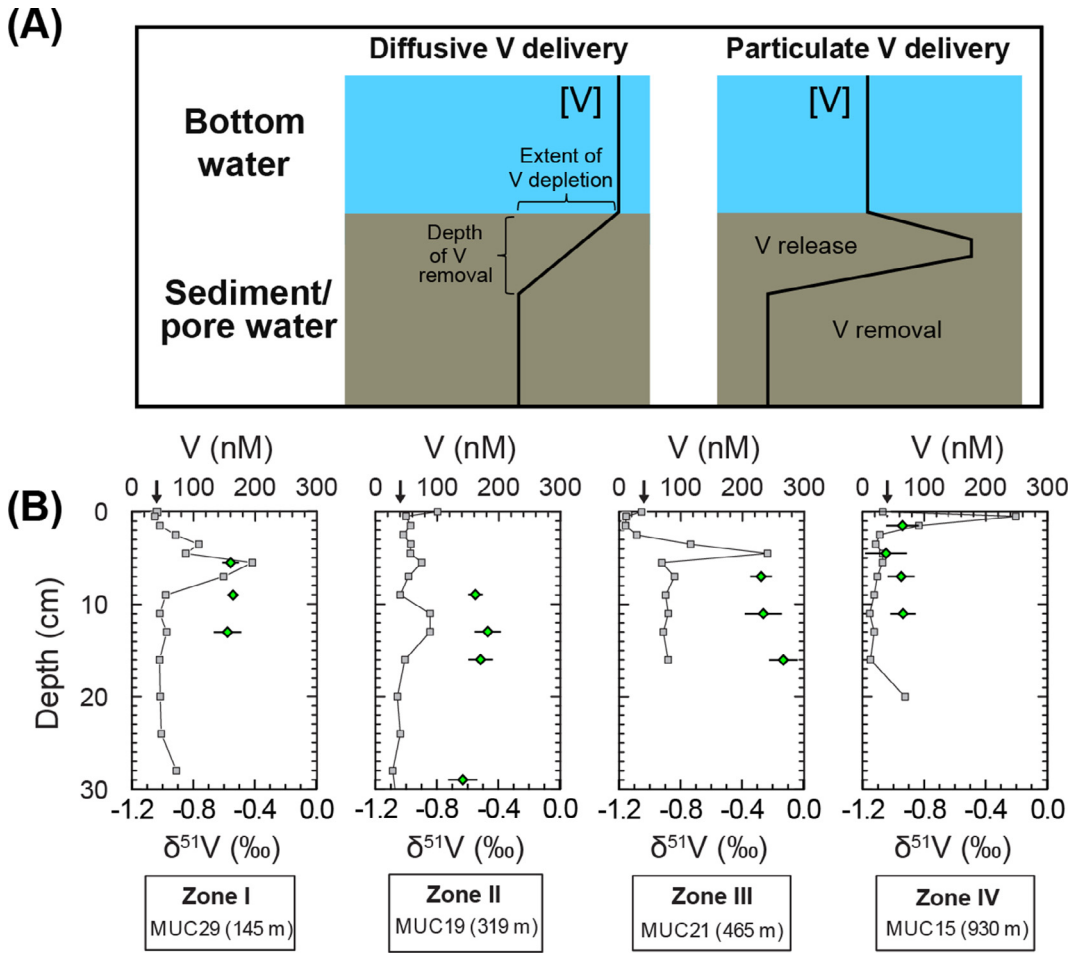

Fig. 7. (A) Generalized representation of pore water V profiles being consistent with different mechanisms of V accumulation made after Scholz et al. (2017): Left figure represents V accumulation through diffusion from the bottom water to the depth of V removal; Right figure represents V release from a solid carrier phase followed by upward diffusion across the sediment water interface and downward diffusion to the depth of V removal. (B) Pore water profiles for [V] in the selected sediment stations on the Peruvian continental margin (grey square), and $\delta^{51}V$ values of the leach proportion for the sediment profile (green dot). Arrows above the upper x-axis indicate average seawater values ([V] sw = 40.3 nM). All the pore water data are from Scholz et al. (2011). (For interpretation of the references to colour in this figure legend, the reader is referred to the web version of this article.)

some of the stations exhibit a distinct peak in V concentration close to the sediment–water interface, which indicates the release of V from solid phases (Fig. 7). This observation would imply that the excess V in the Peruvian margin anoxic sediments is delivered with particulates from the oxygen-deficient seawater column. Additional evidence supporting the particulate delivery mechanism for the V enrichment in anoxic sediments has been documented through the chemical analysis of water column particulate matter, which reveal pronounced V enrichments in the water column within the OMZ (Scholz et al., 2017; Ho et al., 2018). Elevated V concentrations in pore fluids below the sediment–water interface has also been observed for other anoxic continental margin sediments in previous studies (e.g. Brumsack and Gieskes, 1983; Shaw et al., 1990; Morford et al., 2005). Taken together all these observations imply that particulate delivery is the dominant pathway to supply and accumulate V from seawater into anoxic sediments.

If authigenic V enrichment in anoxic sediments is delivered by particulate settling, as discussed above, then the authigenic V isotope composition should reflect the isotope composition of the authigenic V associated with sinking particulates, which ultimately depends on the isotope fractionation between seawater and particulates. Additionally, the final deposited authigenic V isotope composition could also be affected by potential isotope fractionation during remobilization of V from settled particles within the sediment column (e.g. Scholz et al., 2017; Bura-Nakić et al., 2018). For the Peruvian margin sediments, there is no observable down-core V isotope variation for all the stations despite their variable starting bottom O_2 contents and downcore pore water element profiles (Fig. 7 as an example; see more data in Table 5). Thus, any potential remobilization of V from sinking particles appears to cause limited, if any, modification of the initial sedimentary authigenic V isotope signature that is generated in the water column. Instead, it seems more likely that the authigenic V

isotope composition in Peruvian margin sediments depends on the primary authigenic signature associated with sinking particulates, which is mainly controlled by isotope fractionation between V species that bind to particulates and the dissolved V in the seawater.

The isotopic signature of oxic sediments is readily explained in terms of preferential removal of the light V isotopes in the form of vanadate anion (like $H_2VO_4^-$) to Fe-Mn (oxyhydr)oxides due to adsorption as discussed in Section 6.2.1. For comparison, dissolved pentavalent vanadate tends to be reduced to tetravalent vanadyl cation (VO^{2+}) within an oxygen-deficient water column, which can be firmly fixed into particulate organic matter (Szalay and Szilágyi, 1967). Additionally, the general trend of increasing V with organic carbon is observed in particulates collected within Peruvian margin oxygen-deficient seawater (Ohnemus et al., 2017; Ho et al., 2018). Thus, the adsorption of vanadyl into organic particles likely plays an important role in scavenging V from seawater in the oxygen-deficient margins, which should exhibit distinct isotope fractionation factors compared to vanadate bound to Fe-Mn (oxyhydr)oxides. Although delivery of V with Fe (oxyhydr)oxides might also occur within the OMZ (Scholz et al., 2016, 2017; Heller et al., 2017), enrichment of Fe is only observed in the sediments deposited in the oxic bottom waters below the OMZ (Zone IV) where authigenic V display isotope compositions similar to pelagic clays (Fig. 6). Thus, it is more likely that sedimentary V isotope signatures within the OMZ is mainly controlled by the retention of V by organic matter. In conclusion, V isotope fractionation during its removal from seawater likely varies with the speciation and adsorption properties of V in seawater, which is mainly controlled by the local redox environment. The change in authigenic V isotope composition for Peruvian Margin sediments occurring at bottom water oxygen contents of ~ 10 μM might imply that the main phases that bind and scavenge V from seawater to sediments changes from organically bound vanadyl to iron oxyhydroxide adsorbed vanadate around this oxygen threshold.

Previous studies have documented that bottom water oxygen conditions on the Peruvian shelf are driven by fluctuations in the climate and currents with the most intense oxygenation occurring during El Niño periods (Levin et al., 2002; Fuenzalida et al., 2009). Bottom water oxygenation is also occasionally observed in the Santa Barbara Basin (Reimers et al., 1996), which can occur on seasonal and/or interannual time scales driven by oxygenated bottom water renewal (Bograd et al., 2002). Reduced V in the sediments might be re-oxidized to pentavalent V species during transient oxygenation events leading to a destabilization of the authigenic V phases (Wehrli and Stumm, 1989). The occasional bottom water oxygenation could also enhance the carbon turnover and reduce the preservation of refractory organic compounds which could remobilize the metals (e.g. Sun et al., 2002). These factors could mute the authigenic V enrichment and cause remobilization of V in the sediments from the Peruvian shelf (i.e. Zone I) and Santa Barbara Basin. Despite the potential for occasional bottom water oxygenation affecting enrichment patterns, the authigenic V isotope signatures for both sites are similar to those of the Peruvian Margin sediments in the permanently anoxic zones (i.e. Zone II, Fig. 5). Such observations imply that the authigenic V accumulation in these sections mainly occurred during periods of oxygen-deficient bottom water conditions. Further, it seems that re-oxidation of V by short-term fluctuations in bottom water oxygenation might temporarily arrest the V enrichment process, but without changing the authigenic V isotope signature.

Large $\delta^{51}V_{leach}$ variations are observed for the Peruvian Margin sediments from stations in Zone III which were located at the transition between the permanently anoxic and the low oxygen oxic section of the Peruvian margin. In particular, samples from the MUC 21 core document $\delta^{51}V_{leach}$ values of -0.28 to -0.13‰ (Fig. 5), much heavier than other sediments on the continental margin. The observed V isotope fractionation between sediments from MUC 21 and seawater is -0.42 ± 0.22‰. It is noteworthy that the pore water profile observed in MUC 21 documents a drop in vanadium concentrations below the typical bottom seawater value (~40 nM) in the first 3 cm, which indicates the occurrence of a downcore benthic V flux by diffusion (Fig. 7). In addition, previous calculations showed that the downward flux of V is generally consistent with the mass accumulation rates of V for the stations in Zone III (Scholz et al., 2011). Thus, it is likely that the diffusive metal delivery pathway plays a role in controlling the V isotope composition of sediments in MUC 21, and depends on several factors including isotope fractionation factors between reaction species, the extent of element depletion, and the depth over which element removal occurs (e.g. Clark and Johnson, 2008; Andersen et al., 2014). Such effects have been described mathematically using diffusion–reaction-tr ansport models (Clark and Johnson, 2008), which show that the final observed isotopic composition in the sediments will record an integrated composition and that the effective isotope fractionation factor is always smaller than the intrinsic isotope fractionation factor between reactant and product. This is consistent with our observation that the samples from the MUC 21 cores show authigenic V isotope compositions closer to the seawater value as compared to that from other anoxic stations. However, it is unclear why the downward flux of V into the sediment is only observed for stations on the edge of the Peruvian margin OMZ that have low but detectable oxygen in the bottom water (e.g., MUC 21 with bottom water O_2 of 2.1 μM). Further V isotope measurements from pore fluids, the study of additional sedimentary environments, as well as experimental work are required to better constrain the mechanisms controlling the sedimentary V isotope signatures at the boundary between oxic and anoxic water masses.

6.2.3. Euxinic Cariaco Basin

The limited authigenic V isotope variation in the Cariaco Basin, despite the broad basinal coverage and range of water depths from 400 to 1400 m, suggest that V isotope fractionation during authigenic uptake in these sediments is roughly constant across the basin. The observed V isotopic shift between the euxinic sediments in the Cariaco Basin and open-ocean seawater is $\Delta_{eux\text{-}sw} = -0.42 \pm 0.19$‰

(2SD), distinctly smaller than that observed in oxygen-deficient continental margin sediments (-0.70 ± 0.22‰, 2SD). Thus, the removal mechanism of V, that is the removal pathway and/or phase, from sulfidic seawater in the Cariaco Basin might differ from that of oxygen-deficient seawater on the continental margin, which results in different isotope fractionation factors. Or the observed isotopic shift is affected by the local hydrographic conditions, such as the degree of restriction of the subpycnoclinal water masses in the Cariaco Basin.

The delivery pathway of V from seawater into the sediments could affect the observed shift in sedimentary V isotope composition away from seawater. A recent study suggests that the authigenic enrichment of V (calculated relative to Al) for the sinking particulates collected in the Cariaco Basin at various depths below the chemocline is similar to that of core top sediments for the same location (Calvert et al., 2015). In addition, comparing the settling fluxes measured in the deepest traps with the burial fluxes of the underlying laminated sediment shows that V has similar settling and burial fluxes. This is in direct contrast to the behavior of Re and U which all have significantly higher accumulation rates in the modern laminated sediments compared to the modern calculated settling fluxes in the deep Cariaco Basin (Calvert et al., 2015). This observation suggests that the authigenic uptake of V in euxinic sediments from the Cariaco Basin is mainly through particulate delivery occurring in the reducing water column rather than diffusive delivery below the sediment–seawater interface, which is similar to the continental margin oxygen-deficient sediments.

It is thought that the reduction of vanadyl to trivalent V species can occur in the presence of H_2S (Breit and Wanty, 1991). However, experiments conducted by Wanty and Goldhaber (1992) suggest limited production of trivalent V at least on laboratory timescales when the total dissolved sulfide concentration is below 2.3 mM. Additionally, based on paleo-data Scott et al. (2017) suggest that to drive the reduction of V(IV) to V(III), the concentration of H_2S in coeval bottom waters or porewaters must at least exceed 8 mM, which is not found within the modern water column. In addition, the reduction of vanadyl may be inhibited by the high stability of vanadyl-organic complexes that are formed in the water column and sediments, which could increase the stability field of tetravalent vanadyl species relative to pentavalent and trivalent V species (Breit and Wanty, 1991). Additional research on V speciation analysis in sulfidic seawater is required to better understand the isotopic observations. However, given currently available data it appears that the main reduced V species in the Cariaco Basin is likely the tetravalent vanadyl cation (VO^{2+}), which is similar to that expected for the oxygen-deficient seawater in the continental margin.

It is noteworthy that V is depleted in the waters below the chemocline relative to the near-surface depths by ~65% near the center of the Cariaco Basin (Fig. 8, data from Emerson and Huested, 1991), which is due to the slow (~100 years) bottom-water renewal rate in the basin (Deuser, 1973). Previous studies have shown that the observed isotopic shift between the metals accumulated in anoxic sediments and that remaining in seawater also depend on the rate of water renewal versus removal to sediment (e.g. Noordmann et al., 2015; Rolison et al., 2017; Bura-Nakić et al., 2018). Thus, a simple Rayleigh fractionation model (Fig. 9) was constructed to constrain the isotope fractionation during authigenic uptake of V from waters below the chemocline:

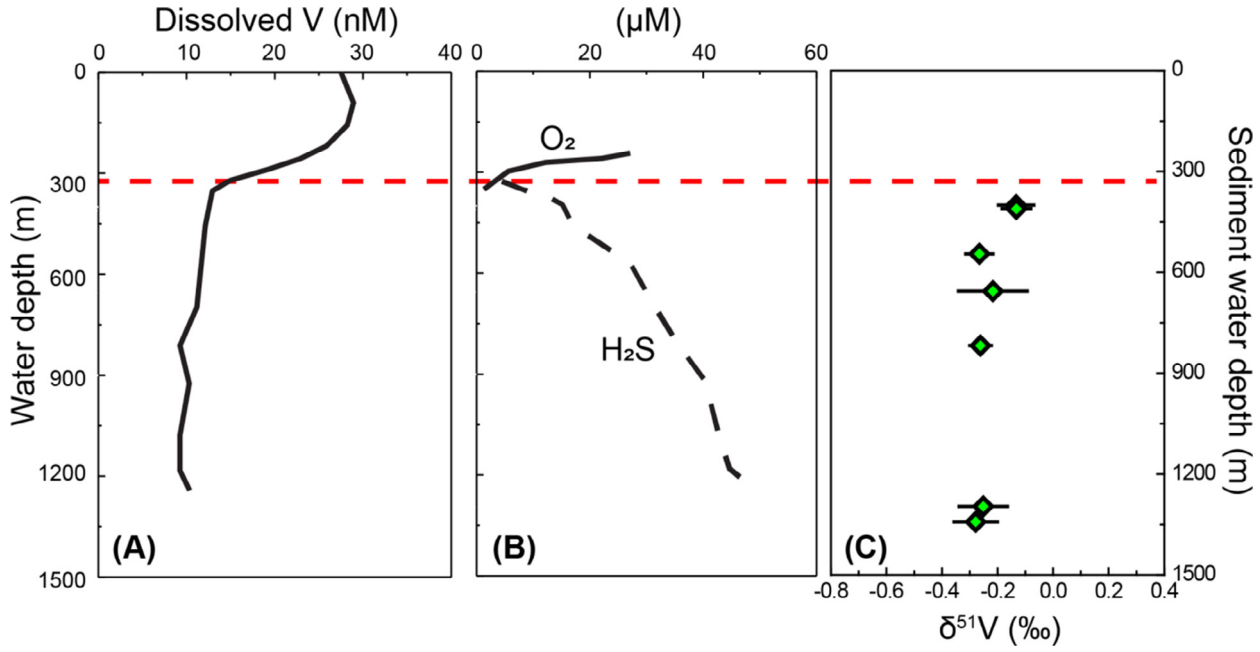

Fig. 8. Water column depth profiles of the concentrations of (A) dissolved V, (B) dissolved O_2 and H_2S in the central Cariaco Basin, and the $\delta^{51}V_{leach}$ values for the Cariaco Basin sediments under various depositional water depths. The water column data are from Emerson and Huested (1991).

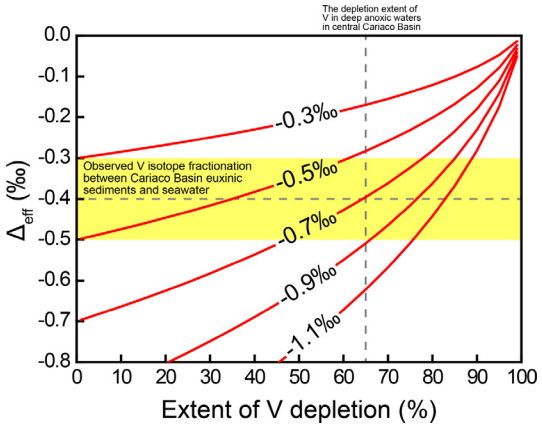

Fig. 9. Model for the Δ_{eff} (effective isotopic fractionation) between V accumulated in sediments and dissolved in seawater in restricted basin with V depletion in deep seawater. Red line shows the Rayleigh fractionation model with different Δ_{int} (intrinsic isotopic fractionation) denoted on the line. The lateral grey dotted line with yellow shadow denotes our observed V isotope fractionation between Cariaco sediments and seawater (-0.4 ± 0.1‰, SD). The vertical grey dotted line denotes the depletion extent of V in the deep anoxic waters of the Cariaco Basin relative to the near-surface depths (see Fig. 8). (For interpretation of the references to colour in this figure legend, the reader is referred to the web version of this article.)

$$\delta_{sea} = (1000 + \delta_{sea0}) \times (1 - f)^{(\alpha-1)} - 1000, \quad (1)$$

where δ_{sea0} and δ_{sea} refer to the isotope composition of V in the initial input seawater ($\delta_{sea0} = 0.2$‰) and remaining after V removal, f refers to the fraction of V removal into sediment, and α is the equilibrium fractionation factor between V in removal phase and seawater. Then the isotope composition of V accumulated in the sediments (δ_{sed}) can be calculated as:

$$\delta_{sed} = (\delta_{sea0} - (1 - f)\delta_{sea})/f. \quad (2)$$

And the effective isotopic fractionation between seawater and sediment (Δ_{eff}) is:

$$\Delta_{eff} = \delta_{sed} - \delta_{sea0}. \quad (3)$$

In this Rayleigh fractionation model, the intrinsic isotopic fractionation ($\Delta_{int} = 1000 \times (\alpha - 1)$) during authigenic uptake of about −0.7‰ is required to explain the observed $\delta^{51}V_{leach}$ values of sediments under anoxic seawater with ~65% depletion of the V inventory for the deep Cariaco Basin (Fig. 9). This fractionation factor is identical to the isotopic fractionation observed in the Peruvian OMZ sediments with water column V depletion of less than 10% (Ho et al., 2018). Given the likely similar V speciation and intrinsic isotope fractionation factors in these two environments, we propose that the removal process of V from mildly sulfidic seawater in the Cariaco Basin is the same as the continental margin oxygen-deficient seawater. If this is the case, our results further indicate that in a restricted euxinic basin, observed $\delta^{51}V$ values could also be influenced by the relationship between the seawater V removal rate and the seawater renewal rate. This explanation for the V isotope compositions of euxinic sediments under moderate sulfidic seawater could be tested with further data from both experimental and natural systems. For example, the analysis of the euxinic sediments from Saanich Inlet, with only 20–40% of V depletion relative to the open ocean seawater (Emerson and Huested, 1991), would be a good place to test the model on the relations between effective isotope shift and deep seawater depletion.

6.3. Implications for the applications of V isotope as a paleo-redox proxy

Our research demonstrates that the authigenic V isotope compositions of marine sediments are directly linked to overlying seawater redox conditions. More importantly, we observe a shift in authigenic V isotope compositions of about 0.4‰ when transitioning from oxic to oxygen-deficient environments (BW O_2 around 10 μM, Fig. 4). Most likely, this isotopic shift records the change of the main phases that bind and scavenge V from seawater that are delivered to sediments around this oxygen threshold. The observed isotopic shift near 10 μM oxygen is unique compared to other currently studied metal isotope systems like Tl, Mo, and U that depend on precipitation with sulfides, reactive-diffusion driven transport and/or possibly Fe-Mn oxide shuttling (e.g. Poulson et al., 2006; Andersen et al., 2014; Nielsen et al., 2017; Scholz et al., 2017; Bura-Nakić et al., 2018; Hardisty et al., 2018). Thus, our study highlights the benefits provided by the V system relative to the handful of other metal isotopes systems being commonly utilized.

In modern oceans, the dominant burial fluxes of V from seawater is thought to be into oxic sediments and hydrothermal sediments that could account > 95% of total buried V, based on the marine flux mass balance estimates by Morford and Emerson (1999). However, the burial of V into anoxic sediments could play an important role for the mass balance of V in ancient oceans, especially during oceanic anoxic events (OAE) when the expansion of marine deoxygenation occurred (e.g. Jenkyns, 2010; Owens et al., 2016; Ostrander et al., 2017), or before the atmospheric oxygen reached near modern levels (e.g. Dahl et al., 2010; Sahoo et al., 2016; Lu et al., 2018). In addition, the long residence time of V (~100 kyrs, Morford and Emerson, 1999) and the occurrence of V isotope differences between at low-oxygen environments (Fig. 4) suggest that V isotope systematics in ancient sediments could become a tool to refine paleo-ocean redox fluctuations. Further quantitative estimates on the oceanic V isotope mass balance require additional studies on the V isotope composition of hydrothermal sediments as these have been estimated as one of the major sinks in the modern ocean (Morford and Emerson, 1999). Most importantly, the unique sensitivity of V isotopes to changes in marine oxygenation around the 10 μM O_2 threshold renders it a potential proxy to better constrain oxygen-deficient environments and provide a more detailed understanding of paleo-ocean oxygenation and deoxygenation events and their associated impacts on marine ecosystems that are hard to constrain with current geochemical or biological proxies.

7. CONCLUSIONS

This study provides the first insights into the variation of V isotope fractionation during the deposition of marine sediments within various redox environments. Our results highlight the direct link between the authigenic V isotope compositions of marine sediments and the overlying local redox conditions. Specifically, the isotope fractionations of V between seawater and the authigenic sediments scale with bottom seawater oxygen concentrations, as summarized in Fig. 4. Authigenic V isotopic compositions of modern marine sediments underlying bottom waters with oxygen contents less than ~10 μM record $\delta^{51}V > -0.7‰$, which is markedly different from that of sediments deposited under bottom water with oxygen contents > 10 μM that exhibit $\delta^{51}V$ values ranging from −1.1 to −0.7‰. This implies that V isotope fractionation during uptake from seawater is sensitive to subtle variations in seafloor oxygen conditions.

This work further provides a framework for the interpretation of V isotope variations in modern sediments. The isotope composition of authigenic V in the oxic sediments is mainly controlled by the isotope fractionation during adsorption of dissolved pentavalent vanadate onto Fe-Mn oxyhydroxide minerals in the sediment. In contrast, V isotope compositions in the sediments deposited under oxygen-deficient seawater likely depends on the isotope fractionation during the accumulation of tetravalent vanadyl into organic-rich particulates primarily within anoxic or euxinic portions of the water column. Additionally, the limited authigenic V isotope variations within sediment profiles, despite their variable sedimentation rates, pore water chemistry, and evidence of V mobilization within the sediment, indicates a lack of V isotope fractionation during early diagenesis and cycling of V. Overall, the shift of authigenic V isotope composition in sediments at bottom water oxygen contents of about 10 μM presumably indicates a change of the main phases that bind and scavenge V from seawater to sediments around this oxygen threshold.

Declaration of Competing Interest

The authors declare that they have no known competing financial interests or personal relationships that could have appeared to influence the work reported in this paper.

ACKNOWLEDGMENT

We would like to thank T. Them and S. Young for providing stimulating conversation on the data from this project. G. White is thanked for instrumentation troubleshooting at the MagLab. The work was funded by grants from NSF-OCE 1434785 (JDO and SGN), and NASA Exobiology NNX16AJ60 (JDO and SGN) and 80NSSC18K1532 (JDO and FW). FS wishes to thank the German Research Foundation (DFG) for funding through Emmy Noether Research Group ICONOX and Collaborative Research Centre 754. CRG acknowledges NSF grants OCE-1234827 & OCE-1235248 (US GEOTRACES). This manuscript has benefited from reviews by Tais W. Dahl, and two anonymous reviewers and the efficient editorial handling from Noah Planavsky.

APPENDIX A. SUPPLEMENTARY MATERIAL

Supplementary data to this article can be found online at https://doi.org/10.1016/j.gca.2020.06.013.

REFERENCES

Abshire M. L., Romaniello S. J., Kuzminov A. M., Cofrancesco J., Severmann S. and Riedinger N. (2020) Uranium isotopes as a proxy for primary depositional redox conditions in organic-rich marine systems. *Earth Planet. Sci. Lett.* **529**, 115878.

Algeo T. J. (2004) Can marine anoxic events draw down the trace element inventory of seawater? *Geology* **32**, 1057–1060.

Algeo T. J. and Li C. (2020) Redox classification and calibration of redox thresholds in sedimentary systems. *Geochim. Cosmochim. Acta*.

Algeo T. J. and Maynard J. B. (2004) Trace-element behavior and redox facies in core shales of Upper Pennsylvanian Kansas-type cyclothems. *Chem. Geol.* **206**, 289–318.

Algeo T. J. and Tribovillard N. (2009) Environmental analysis of paleoceanographic systems based on molybdenum–uranium covariation. *Chem. Geol.* **268**, 211–225.

Anbar A. D. and Rouxel O. (2007) Metal stable isotopes in paleoceanography. *Annu. Rev. Earth Pl. Sc.* **35**, 717–746.

Andersen M. B., Romaniello S., Vance D., Little S. H., Herdman R. and Lyons T. W. (2014) A modern framework for the interpretation of 238U/235U in studies of ancient ocean redox. *Earth Planet. Sci. Lett.* **400**, 184–194.

Bernhard J. M. and Reimers C. E. (1991) Benthic foraminiferal population fluctuations related to anoxia: Santa Barbara Basin. *Biogeochemistry* **15**, 127–149.

Bernhard J. M., Sen Gupta B. K. and Borne P. F. (1997) Benthic foraminiferal proxy to estimate dysoxic bottom-water oxygen concentrations; Santa Barbara Basin, US Pacific continental margin. *J. Foraminiferal Res.* **27**, 301–310.

Bischoff J. L., Heath G. R. and Leinen M. (1979) Geochemistry of deep-sea sediments from the Pacific manganese nodule province: DOMES Sites A, B, and C, Marine geology and oceanography of the Pacific manganese nodule province. *Springer*, 397–436.

Bograd S. J., Schwing F. B., Castro C. G. and Timothy D. A. (2002) Bottom water renewal in the Santa Barbara Basin. *J. Geophys. Res. Oceans* **107**, 9-1-9-9.

Bonatti E., Fisher D., Joensuu O. and Rydell H. (1971) Postdepositional mobility of some transition elements, phosphorus, uranium and thorium in deep sea sediments. *Geochim. Cosmochim. Acta* **35**, 189–201.

Böning P., Brumsack H.-J., Böttcher M. E., Schnetger B., Kriete C., Kallmeyer J. and Borchers S. L. (2004) Geochemistry of Peruvian near-surface sediments. *Geochim. Cosmochim. Acta* **68**, 4429–4451.

Breit G. N. and Wanty R. B. (1991) Vanadium accumulation in carbonaceous rocks - a review of geochemical controls during deposition and diagenesis. *Chem. Geol.* **91**, 83–97.

Brumsack H. J. and Gieskes J. M. (1983) Interstitial water trace-metal chemistry of laminated sediments from the Gulf of California, Mexico. *Mar. Chem.* **14**, 89–106.

Bura-Nakić E., Andersen M. B., Archer C., de Souza G. F., Marguš M. and Vance D. (2018) Coupled Mo-U abundances and isotopes in a small marine euxinic basin: Constraints on

processes in euxinic basins. *Geochim. Cosmochim. Acta* **222**, 212–229.
Calvert S., Piper D., Thunell R. and Astor Y. (2015) Elemental settling and burial fluxes in the Cariaco Basin. *Mar. Chem.* **177**, 607–629.
Canfield D. E., Raiswell R. and Bottrell S. H. (1992) The reactivity of sedimentary iron minerals toward sulfide. *Am. J. Sci.* **292**, 659–683.
Chester R. and Hughes M. (1967) A chemical technique for the separation of ferro-manganese minerals, carbonate minerals and adsorbed trace elements from pelagic sediments. *Chem. Geol.* **2**, 249–262.
Chiessi C. M., Ulrich S., Mulitza S., Pätzold J. and Wefer G. (2007) Signature of the Brazil-Malvinas Confluence (Argentine Basin) in the isotopic composition of planktonic foraminifera from surface sediments. *Mar. Micropaleontol.* **64**, 52–66.
Clark S. K. and Johnson T. M. (2008) Effective isotopic fractionation factors for solute removal by reactive sediments: a laboratory microcosm and slurry study. *Environ. Sci. Technol.* **42**, 7850–7855.
Collier R. W. (1984) Particulate and dissolved vanadium in the North Pacific Ocean. *Nature* **309**, 441–444.
Crusius J., Calvert S., Pedersen T. and Sage D. (1996) Rhenium and molybdenum enrichments in sediments as indicators of oxic, suboxic and sulfidic conditions of deposition. *Earth Planet. Sci. Lett.* **145**, 65–78.
Dahl T. W., Hammarlund E. U., Anbar A. D., Bond D. P., Gill B. C., Gordon G. W., Knoll A. H., Nielsen A. T., Schovsbo N. H. and Canfield D. E. (2010) Devonian rise in atmospheric oxygen correlated to the radiations of terrestrial plants and large predatory fish. *Proc. Natl. Acad. Sci.* **107**, 17911–17915.
Deuser W. G. (1973) Cariaco Trench: oxidation of organic matter and residence time of anoxic water. *Nature* **242**, 601.
Dunlea A. G., Murray R. W., Sauvage J., Spivack A. J., Harris R. N. and D'Hondt S. (2015) Dust, volcanic ash, and the evolution of the South Pacific Gyre through the Cenozoic. *Paleoceanogr. Paleoclimatol.* **30**, 1078–1099.
Emerson S. R. and Huested S. S. (1991) Ocean anoxia and the concentrations of molybdenum and vanadium in seawater. *Mar. Chem.* **34**, 177–196.
Filippidi A. and De Lange G. (2019) Eastern mediterranean deep water formation during sapropel S1: A reconstruction using geochemical records along a bathymetric transect in the adriatic outflow region. *Paleoceanogr. Paleoclimatol.* **34**, 409–429.
Fuenzalida R., Schneider W., Garcés-Vargas J., Bravo L. and Lange C. (2009) Vertical and horizontal extension of the oxygen minimum zone in the eastern South Pacific Ocean. *Deep Sea Res. Part II* **56**, 992–1003.
Han T., Fan H. and Wen H. (2018) Dwindling vanadium in seawater during the early Cambrian, South China. *Chem. Geol.* **492**, 20–29.
Hardisty D. S., Lyons T. W., Riedinger N., Isson T. T., Owens J. D., Aller R. C., Rye D. M., Planavsky N. J., Reinhard C. T., Gill B. C., Masterson A. L., Asael D. and Johnston D. T. (2018) An evaluation of sedimentary molybdenum and iron as proxies for pore fluid paleoredox conditions. *Am. J. Sci.* **318**, 527–556.
Heller M. I., Lam P. J., Moffett J. W., Till C. P., Lee J.-M., Toner B. M. and Marcus M. A. (2017) Accumulation of Fe oxyhydroxides in the Peruvian oxygen deficient zone implies non-oxygen dependent Fe oxidation. *Geochim. Cosmochim. Acta* **211**, 174–193.
Ho P., Lee J.-M., Heller M. I., Lam P. J. and Shiller A. M. (2018) The distribution of dissolved and particulate Mo and V along the US GEOTRACES East Pacific Zonal Transect (GP16): The roles of oxides and biogenic particles in their distributions in the oxygen deficient zone and the hydrothermal plume. *Mar. Chem.* **201**, 242–255.
Hopkins S. S., Prytulak Juli, Barling Jan, Russell S. S., Coles B. J. and Halliday A. N. (2019) The vanadium isotopic composition of lunar basalts. *Earth and Planetary Science Letters* **511**, 12–24.
Inthorn M., Wagner T., Scheeder G. and Zabel M. (2006) Lateral transport controls distribution, quality, and burial of organic matter along continental slopes in high-productivity areas. *Geology* **34**, 205–208.
Jeandel C., Caisso M. and Minster J. F. (1987) Vanadium behaviour in the global ocean and in the Mediterranean sea. *Mar. Chem.* **21**, 51–74.
Jenkyns H. C. (2010) Geochemistry of oceanic anoxic events. *Geochem. Geophys., Geosyst.*, 11.
Kendall B., Dahl T. W. and Anbar A. D. (2017) The stable isotope geochemistry of molybdenum. *Rev. Mineral. Geochem.* **82**, 683–732.
Koschinsky A., Winkler A. and Fritsche U. (2003) Importance of different types of marine particles for the scavenging of heavy metals in the deep-sea bottom water. *Appl. Geochem.* **18**, 693–710.
Krastel, S., Wefer, G.., 2012. Report and preliminary results of RV METEOR Cruise M78/3. Sediment transport off Uruguay and Argentina: From the shelf to the deep sea. 19.05.2009 – 06.07.2009, Montevideo (Uruguay) – Montevideo (Uruguay). Berichte, Fachbereich Geowissenschaften, Universität Bremen, No. 285, 79 pages. Bremen.
Krastel S., Wefer G., Hanebuth T. J., Antobreh A. A., Freudenthal T., Preu B., Schwenk T., Strasser M., Violante R. and Winkelmann D. (2011) Sediment dynamics and geohazards off Uruguay and the de la Plata River region (northern Argentina and Uruguay). *Geo-Mar. Lett.* **31**, 271–283.
Levin L. (2003) Oxygen minimum zone benthos: adaptation and community response to hypoxia. *Oceanography Mar. Biol.: Annual Rev.*.
Levin L., Gutiérrez D., Rathburn A., Neira C., Sellanes J., Munoz P., Gallardo V. and Salamanca M. (2002) Benthic processes on the Peru margin: a transect across the oxygen minimum zone during the 1997–98 El Niño. *Prog. Oceanogr.* **53**, 1–27.
Lu, W., Ridgwell, A., Thomas, E., Hardisty, D.S., Luo, G., Algeo, T.J., Saltzman, M.R., Gill, B.C., Shen, Y., Ling, H.-F., 2018. Late inception of a resiliently oxygenated upper ocean. Science, eaar5372.
McCaffrey M. A., Farrington J. W. and Repeta D. J. (1990) The organic geochemistry of Peru margin surface sediments: I. A comparison of the C37 alkenone and historical El Niño records. *Geochimica et Cosmochimica Acta* **54**(6), 1671–1682.
McManus J., Berelson W. M., Severmann S., Poulson R. L., Hammond D. E., Klinkhammer G. P. and Holm C. (2006) Molybdenum and uranium geochemistry in continental margin sediments: paleoproxy potential. *Geochim. Cosmochim. Acta* **70**, 4643–4662.
Meyer K. M. and Kump L. R. (2008) Oceanic euxinia in earth history: causes and consequences. *Annu. Rev. Earth Pl. Sc.* **36**, 251–288.
Mills D. B., Ward L. M., Jones C., Sweeten B., Forth M., Treusch A. H. and Canfield D. E. (2014) Oxygen requirements of the earliest animals. *Proc. Natl. Acad. Sci.* **111**, 4168–4172.
Moffitt S. E., Hill T. M., Ohkushi K., Kennett J. P. and Behl R. J. (2014) Vertical oxygen minimum zone oscillations since 20 ka in Santa Barbara Basin: A benthic foraminiferal community perspective. *Paleoceanography* **29**, 44–57.
Morford J., Emerson S., Breckel E. and Kim S. (2005) Diagenesis of oxyanions (V, U, Re, and Mo) in pore waters and sediments from a continental margin. *Geochim. Cosmochim. Acta* **69**, 5021–5032.

Morford J. L. and Emerson S. (1999) The geochemistry of redox sensitive trace metals in sediments. *Geochim. Cosmochim. Acta* **63**, 1735–1750.

Nameroff T. J., Balistrieri L. S. and Murray J. W. (2002) Suboxic trace metal geochemistry in the Eastern Tropical North Pacific. *Geochim. Cosmochim. Acta* **66**, 1139–1158.

Nielsen S. G., Auro M., Righter K., Davis D., Prytulak J., Wu F. and Owens J. D. (2019) Nucleosynthetic vanadium isotope heterogeneity of the early solar system recorded in chondritic meteorites. *Earth Planet. Sci. Lett.* **505**, 131–140.

Nielsen S. G., Owens J. D. and Horner T. J. (2016) Analysis of high-precision vanadium isotope ratios by medium resolution MC-ICP-MS. *J. Anal. At. Spectrom.* **31**, 531–536.

Nielsen S. G., Prytulak J. and Halliday A. N. (2011) Determination of precise and accurate 51V/50V isotope ratios by MC-ICP-MS, part 1: chemical separation of vanadium and mass spectrometric protocols. *Geostand. Geoanal. Res.* **35**, 293–306.

Nielsen S. G., Rehkämper M. and Prytulak J. (2017) Investigation and Application of Thallium Isotope Fractionation. *Rev. Mineral. Geochem.* **82**, 759–798.

Noordmann J., Weyer S., Montoya-Pino C., Dellwig O., Neubert N., Eckert S., Paetzel M. and Böttcher M. E. (2015) Uranium and molybdenum isotope systematics in modern euxinic basins: Case studies from the central Baltic Sea and the Kyllaren fjord (Norway). *Chem. Geol.* **396**, 182–195.

Ohnemus D. C., Rauschenberg S., Cutter G. A., Fitzsimmons J. N., Sherrell R. M. and Twining B. S. (2017) Elevated trace metal content of prokaryotic communities associated with marine oxygen deficient zones. *Limnol. Oceanogr.* **62**, 3–25.

Ostrander C. M., Owens J. D. and Nielsen S. G. (2017) Constraining the rate of oceanic deoxygenation leading up to a Cretaceous Oceanic Anoxic Event (OAE-2:∼ 94 Ma). *Sci. Adv.* **3**, e1701020.

Owens J. D. (2019) *Application of Thallium Isotopes: Tracking Marine Oxygenation through Manganese Oxide Burial*. Cambridge University Press.

Owens J. D., Nielsen S. G., Horner T. J., Ostrander C. M. and Peterson L. C. (2017) Thallium-isotopic compositions of euxinic sediments as a proxy for global manganese-oxide burial. *Geochim. Cosmochim. Acta* **213**, 291–307.

Owens J. D., Reinhard C. T., Rohrssen M., Love G. D. and Lyons T. W. (2016) Empirical links between trace metal cycling and marine microbial ecology during a large perturbation to Earth's carbon cycle. *Earth Planet. Sci. Lett.* **449**, 407–417.

Pennington J. T., Mahoney K. L., Kuwahara V. S., Kolber D. D., Calienes R. and Chavez F. P. (2006) Primary production in the eastern tropical Pacific: A review. *Prog. Oceanogr.* **69**, 285–317.

Peterson, L.C., Overpeck, J.T., Murray, D.W., 1990. A High-Resolution Paleoenvironmental Study of the Cariaco Basin, Venezuela: Late Quaternary to Present - Preliminary Report on R/V Thomas Washington Cruise PLUME-07. RSMAS/ University of Miami Technical Report: 50.

Peterson R. G. and Stramma L. (1991) Upper-level circulation in the South Atlantic Ocean. *Prog. Oceanogr.* **26**, 1–73.

Piper D. and Calvert S. (2009) A marine biogeochemical perspective on black shale deposition. *Earth Sci. Rev.* **95**, 63–96.

Poulson R. L., Siebert C., McManus J. and Berelson W. M. (2006) Authigenic molybdenum isotope signatures in marine sediments. *Geology* **34**, 617–620.

Poulton S. W. and Canfield D. E. (2011) Ferruginous conditions: a dominant feature of the ocean through Earth's history. *Elements* **7**, 107–112.

Prytulak J., Nielsen S. G. and Halliday A. N. (2011) Determination of precise and accurate 51V/50V isotope ratios by multi-collector ICP-MS, Part 2: isotopic composition of six reference materials plus the allende chondrite and verification tests. *Geostand. Geoanal. Res.* **35**, 307–318.

Prytulak J., Sossi P. A., Halliday A. N., Plank T., Savage P. S. and Woodhead J. D. (2017) Stable vanadium isotopes as a redox proxy in magmatic systems? *Geochem. Perspect. Lett.* **3**, 75–84.

Qi Y.-H., Wu F., Ionov D. A., Puchtel I. S., Carlson R. W., Nicklas R. W., Yu H.-M., Kang J.-T., Li C.-H. and Huang F. (2019) Vanadium isotope composition of the Bulk Silicate Earth: constraints from peridotites and komatiites. *Geochim. Cosmochim. Acta* **259**, 288–301.

Raiswell R., Buckley F., Berner R. A. and Anderson T. (1988) Degree of pyritization of iron as a paleoenvironmental indicator of bottom-water oxygenation. *J. Sediment. Res.* **58**, 812–819.

Raiswell R. and Canfield D. E. (1998) Sources of iron for pyrite formation in marine sediments. *Am. J. Sci.* **298**, 219–245.

Raiswell R., Hardisty D. S., Lyons T. W., Canfield D. E., Owens J. D., Planavsky N. J., Poulton S. W. and Reinhard C. T. (2018) The iron paleoredox proxies: A guide to the pitfalls, problems and proper practice. *Am. J. Sci.* **318**, 491–526.

Reimers C. E., Lange C. B., Tabak M. and Bernhard J. M. (1990) Seasonal spillover and varve formation in the Santa Barbara Basin, California. *Limnol. Oceanogr.* **35**, 1577–1585.

Reimers C. E., Ruttenberg K. C., Canfield D. E., Christiansen M. B. and Martin J. B. (1996) Porewater pH and authigenic phases formed in the uppermost sediments of the Santa Barbara Basin. *Geochim. Cosmochim. Acta* **60**, 4037–4057.

Reinhard, C.T., Planavsky, N.J., Olson, S.L., Lyons, T.W., Erwin, D.H., 2016. Earth's oxygen cycle and the evolution of animal life. Proc. Natl. Acad. Sci., 201521544.

Reinhard C. T., Planavsky N. J., Wang X., Fischer W. W., Johnson T. M. and Lyons T. W. (2014) The isotopic composition of authigenic chromium in anoxic marine sediments: A case study from the Cariaco Basin. *Earth Planet. Sci. Lett.* **407**, 9–18.

Rolison J. M., Stirling C. H., Middag R. and Rijkenberg M. J. (2017) Uranium stable isotope fractionation in the Black Sea: Modern calibration of the 238 U/235 U paleo-redox proxy. *Geochim. Cosmochim. Acta* **203**, 69–88.

Rudnick R. and Gao S. (2003) Composition of the continental crust. *Treatise Geochem.* **3**, 1–64.

Sahoo S. K., Planavsky N. J., Jiang G., Kendall B., Owens J. D., Wang X., Shi X., Anbar A. D. and Lyons T. W. (2016) *Oceanic oxygenation events in the anoxic Ediacaran ocean*. Geobiology, n/a-n/a.

Sahoo S. K., Planavsky N. J., Kendall B., Wang X., Shi X., Scott C., Anbar A. D., Lyons T. W. and Jiang G. (2012) Ocean oxygenation in the wake of the Marinoan glaciation. *Nature* **489**, 546–549.

Schimmelmann A., Hendy I. L., Dunn L., Pak D. K. and Lange C. B. (2013) Revised∼ 2000-year chronostratigraphy of partially varved marine sediment in Santa Barbara Basin, California. *GFF* **135**, 258–264.

Scholz F. (2018) Identifying oxygen minimum zone-type biogeochemical cycling in Earth history using inorganic geochemical proxies. *Earth Sci. Rev.*.

Scholz F., Hensen C., Noffke A., Rohde A., Liebetrau V. and Wallmann K. (2011) Early diagenesis of redox-sensitive trace metals in the Peru upwelling area–response to ENSO-related oxygen fluctuations in the water column. *Geochim. Cosmochim. Acta* **75**, 7257–7276.

Scholz F., Löscher C. R., Fiskal A., Sommer S., Hensen C., Lomnitz U., Wuttig K., Göttlicher J., Kossel E. and Steininger R. (2016) Nitrate-dependent iron oxidation limits iron transport in anoxic ocean regions. *Earth Planet. Sci. Lett.* **454**, 272–281.

Scholz F., Severmann S., McManus J. and Hensen C. (2014a) Beyond the Black Sea paradigm: The sedimentary fingerprint of an open-marine iron shuttle. *Geochim. Cosmochim. Acta* **127**, 368–380.

Scholz F., Severmann S., McManus J., Noffke A., Lomnitz U. and Hensen C. (2014b) On the isotope composition of reactive iron in marine sediments: Redox shuttle versus early diagenesis. *Chem. Geol.* **389**, 48–59.

Scholz F., Siebert C., Dale A. W. and Frank M. (2017) Intense molybdenum accumulation in sediments underneath a nitrogenous water column and implications for the reconstruction of paleo-redox conditions based on molybdenum isotopes. *Geochim. Cosmochim. Acta* **213**, 400–417.

Schuth S., Brüske A., Hohl S. V., Jiang S.-Y., Meinhardt A.-K., Gregory D. D., Viehmann S. and Weyer S. (2019) Vanadium and its isotope composition of river water and seawater: Analytical improvement and implications for vanadium isotope fractionation. *Chem. Geol.* **528**, 119261.

Schuth S., Horn I., Brüske A., Wolff P. E. and Weyer S. (2017) First vanadium isotope analyses of V-rich minerals by femtosecond laser ablation and solution-nebulization MC-ICP-MS. *Ore Geol. Rev.* **81**, 1271–1286.

Scott C. and Lyons T. W. (2012) Contrasting molybdenum cycling and isotopic properties in euxinic versus non-euxinic sediments and sedimentary rocks: refining the paleoproxies. *Chem. Geol.* **324**, 19–27.

Scott C., Slack J. F. and Kelley K. D. (2017) The hyper-enrichment of V and Zn in black shales of the Late Devonian-Early Mississippian Bakken Formation (USA). *Chem. Geol.* **452**, 24–33.

Scranton M. I., Astor Y., Bohrer R., Ho T.-Y. and Muller-Karger F. (2001) Controls on temporal variability of the geochemistry of the deep Cariaco Basin. *Deep Sea Res. Part I* **48**, 1605–1625.

Shannon L. and Nelson G. (1996) The Benguela: large scale features and processes and system variability. *The south atlantic. Springer*, 163–210.

Shaw T. J., Gieskes J. M. and Jahnke R. A. (1990) Early diagenesis in differing depositional environments: The response of transition metals in pore water. *Geochim. Cosmochim. Acta* **54**, 1233–1246.

Shiller A. M. and Boyle E. A. (1987) Dissolved Vanadium in Rivers and Estuaries. *Earth Planet. Sci. Lett.* **86**, 214–224.

Sholkovitz E. (1973) Interstitial water chemistry of the Santa Barbara Basin sediments. *Geochim. Cosmochim. Acta* **37**, 2043–2073.

Sossi P. A., Prytulak J. and O'Neill H. S. C. (2018) Experimental calibration of vanadium partitioning and stable isotope fractionation between hydrous granitic melt and magnetite at 800 C and 0.5 GPa. *Contributions to Mineralogy and Petrology* **173**(4), 27.

Sperling E. A., Frieder C. A., Raman A. V., Girguis P. R., Levin L. A. and Knoll A. H. (2013) Oxygen, ecology, and the Cambrian radiation of animals. *Proc. Natl. Acad. Sci.* **110**, 13446–13451.

Sperling E. A., Knoll A. H. and Girguis P. R. (2015) The ecological physiology of Earth's second oxygen revolution. *Annu. Rev. Ecol. Evol. Syst.* **46**, 215–235.

Suess E. and von Huene R. (1988) Ocean drilling program leg 112, Peru continental margin: Part 2, Sedimentary history and diagenesis in a coastal upwelling environment. *Geology* **16**, 939–943.

Sun M.-Y., Aller R. C., Lee C. and Wakeham S. G. (2002) Effects of oxygen and redox oscillation on degradation of cell-associated lipids in surficial marine sediments. *Geochim. Cosmochim. Acta* **66**, 2003–2012.

Szalay A. and Szilágyi M. (1967) The association of vanadium with humic acids. *Geochim. Cosmochim. Acta* **31**, 1–6.

Tribovillard N., Algeo T. J., Lyons T. and Riboulleau A. (2006) Trace metals as paleoredox and paleoproductivity proxies: An update. *Chem. Geol.* **232**, 12–32.

Tyson R. V. and Pearson T. H. (1991) Modern and ancient continental shelf anoxia: an overview. *Geological Society, London, Special Publications* **58**, 1–24.

Wanty R. B. and Goldhaber M. B. (1992) Thermodynamics and kinetics of reactions involving vanadium in natural systems: Accumulation of vanadium in sedimentary rocks. *Geochim. Cosmochim. Acta* **56**, 1471–1483.

Wehrli B. and Stumm W. (1989) Vanadyl in natural waters: Adsorption and hydrolysis promote oxygenation. *Geochim. Cosmochim. Acta* **53**, 69–77.

Wu F., Owens J. D., Huang T., Sarafian A., Huang K.-F., Sen I. S., Horner T. J., Blusztajn J., Morton P. and Nielsen S. G. (2019a) Vanadium isotope composition of seawater. *Geochim. Cosmochim. Acta* **244**, 403–415.

Wu F., Owens J. D., Tang L., Dong Y. and Huang F. (2019b) Vanadium isotopic fractionation during the formation of marine ferromanganese crusts and nodules. *Geochimica et Cosmochimica Acta* **265**, 371–385.

Wu F., Qi Y., Perfit M. R., Gao Y., Langmuir C. H., Wanless V. D., Yu H. and Huang F. (2018) Vanadium isotope compositions of mid-ocean ridge lavas and altered oceanic crust. *Earth Planet. Sci. Lett.* **493**, 128–139.

Wu F., Qi Y., Yu H., Tian S., Hou Z. and Huang F. (2016) Vanadium isotope measurement by MC-ICP-MS. *Chem. Geol.* **421**, 17–25.

Wu F., Qin T., Li X., Liu Y., Huang J.-H., Wu Z. and Huang F. (2015) First-principles investigation of vanadium isotope fractionation in solution and during adsorption. *Earth Planet. Sci. Lett.* **426**, 216–224.

Zheng Y., Anderson R. F., van Geen A. and Fleisher M. Q. (2002) Preservation of particulate non-lithogenic uranium in marine sediments. *Geochim. Cosmochim. Acta* **66**, 3085–3092.

Zheng Y., Anderson R. F., van Geen A. and Kuwabara J. (2000) Authigenic molybdenum formation in marine sediments: a link to pore water sulfide in the Santa Barbara Basin. *Geochim. Cosmochim. Acta* **64**, 4165–4178.

Zabel, M., 2003. Report and preliminary results of METEOR Cruise M 57/2, Walvis Bay – Walvis Bay, 11.02. – 12.03.2003. Berichte, Fachbereich Geowissenschaften, Universität Bremen, No. 220, 136 pages, Bremen.

Associate editor: Noah J. Planavsky